

Julian Skrotzki

Nonstandard neutrino oscillations and the IceCube experiment

Erweiterte Neutrinooszillationsmodelle
und das IceCube-Experiment

Diplomarbeit

Institut für Theoretische Physik
Universität Karlsruhe

März 2008

Referent: Prof. Dr. F. R. Klinkhamer (ITP)
Korreferent: Prof. Dr. G. Drexlin (EKP)

Ich versichere, dass ich diese Arbeit selbständig verfasst und keine anderen als die angegebenen Hilfsmittel verwendet habe.

Julian Skrotzki
Karlsruhe, 17. März 2008

Als Diplomarbeit anerkannt.

Prof. Dr. Frans R. Klinkhamer
Karlsruhe, 17. März 2008

Contents

1	Introduction	1
1.1	History of neutrino physics	1
1.2	Standard model of elementary particle physics	2
1.3	Neutrino oscillations	3
1.4	Outlook	4
2	Standard mass-difference neutrino oscillations	5
2.1	General neutrino-oscillation probability	6
2.2	Two-flavor case	7
2.3	Three-flavor case	8
2.4	CP, T, and CPT invariances	11
3	Ultrahigh-energy cosmic rays and cosmogenic neutrinos	13
3.1	Possible origin of ultrahigh-energy cosmic rays	13
3.1.1	Neutron stars	14
3.1.2	Active galactic nuclei and radio galaxies	15
3.1.3	Gamma ray bursts	16
3.2	Cosmic microwave, ultraviolet-optical, and infrared backgrounds	17
3.3	Greisen–Zatsepin–Kuzmin mechanism	18
3.4	Cosmic ray scattering off the cosmic UV-optical and infrared backgrounds	20
3.5	Energy spectrum of high-energy cosmogenic neutrinos	21
4	IceCube experiment	23
4.1	Tau neutrino events in the IceCube experiment	23
4.1.1	Double-bang signature	25
4.1.2	Lollipop signature	26
4.1.3	Inverted-lollipop signature	26
4.1.4	Sugardaddy signature	26
5	Standard mass-difference neutrino oscillations and IceCube	29
6	Nonstandard neutrino oscillations and IceCube	31

7 Conclusion	47
A GZK kinematics	49
Bibliography	51
Acknowledgments	53
Zusammenfassung	55

Chapter 1

Introduction

This work will be concerned with neutrino physics and, in particular, with neutrino oscillations. Therefore, a short introduction into the history of neutrino physics, the standard model of particle physics and neutrino oscillations will be given in this chapter. It is followed by a brief outlook on the subsequent chapters. From now on, the convention $\hbar = c = 1$ will be used.

1.1 History of neutrino physics

In 1930, Wolfgang Pauli postulated the existence of a new particle, a neutral fermion with spin $1/2$ and small mass, which he called the “neutron”, in order to describe the continuous spectrum of the β -decay process

$${}^A_Z X \rightarrow {}^A_{Z+1} Y + e^- + \bar{\nu}_e. \quad (1.1)$$

If no antineutrino took part in the decay process, the energy spectrum of the electron would have to be discrete and its energy would be the energy difference between ${}^A_Z X$ and ${}^A_{Z+1} Y$. Furthermore, without the presence of the antineutrino, angular momentum would not be conserved. In 1932, James Chadwick discovered the particle now known as the neutron. It was clear that this particle could not be the same as the particle which had been postulated by Pauli, since Pauli’s “neutron” could at most have the mass of one percent of the proton mass. Therefore, Pauli’s “neutron” was given the new name “neutrino” by Fermi in 1933. In the same year, it was concluded that the neutrino had to be massless and in the following year, Fermi presented his theory of β -decay. It was very difficult to detect the neutrino in experiments directly due to the extreme smallness of neutrino interaction cross-sections. Thus, it took until 1956

that the existence of the electron neutrino could be verified experimentally by Clyde L. Cowan Jr. and Frederick Reines by means of the inverse β -decay process

$$\bar{\nu}_e + p \rightarrow n + e^+. \quad (1.2)$$

In 1962, Leon M. Lederman, Melvin Schwartz, and Jack Steinberger detected the muon neutrino. The first direct detection of the tau neutrino was announced by the DONUT collaboration at Fermilab in 2000.

Neutrino-oscillation experiments started in the late 1960s. One of the first experiments which observed the oscillation of solar neutrinos was the Homestake experiment by Raymond Davis Jr. It operated from 1970 until 1994. In the late 1990s, more accurate neutrino-oscillation experiments such as the Sudbury Neutrino Observatory and Super-Kamiokande began to measure the neutrino-oscillation parameters. This is a still ongoing process with new experiments trying to advance previous experimental results.

1.2 Standard model of elementary particle physics

The standard model of elementary particle physics (SM) is the theory which describes the fundamental forces of strong, weak, and electromagnetic interactions and the fundamental fermionic particles of which all matter consists. The fundamental fermions are arranged in two different groups, the quarks, which have color charge and can interact via the strong force, and the leptons, which do not have color charge and cannot interact via the strong force. The quarks and leptons are divided into three generations, where each quark and lepton has a partner in the other two generations. These partners have the same properties but very different masses. The masses of the particles increase from generation to generation, which means that the fundamental fermions in the first generation are the lightest ones and therefore stable. In the quark sector, the three generations are

$$\begin{pmatrix} u \\ d \end{pmatrix}, \begin{pmatrix} c \\ s \end{pmatrix}, \begin{pmatrix} t \\ b \end{pmatrix}, \quad (1.3)$$

where u is the up quark, d the down quark, s the strange quark, c the charm quark, b the bottom quark, and t the top quark (in order of their masses). More precisely, these are the fields standing for the respective particles. In the lepton sector, the generations are

$$\begin{pmatrix} e \\ \nu_e \end{pmatrix}, \begin{pmatrix} \mu \\ \nu_\mu \end{pmatrix}, \begin{pmatrix} \tau \\ \nu_\tau \end{pmatrix}, \quad (1.4)$$

where e is the electron, ν_e the electron neutrino, μ the muon, ν_μ the muon neutrino, τ the tau, and ν_τ the tau neutrino. Again, to be more precise, these are the fields which stand for the respective particles.

The quarks carry an electric charge of $+2/3$ (up, charm, and top quark) or $-1/3$ (down, strange, and bottom quark). The charged leptons, i.e. electron, muon, and tau,

carry an electric charge of -1 , whereas the neutrinos do not carry any electric charge. The corresponding antiparticles to the quarks and leptons carry the negative electric charge of the particles.

Within the SM, the fundamental forces are mediated by gauge bosons. These are the photon for the electromagnetic force, the W^\pm and Z^0 for the weak force, and eight gluons for the strong force, summing up to a total of twelve gauge bosons. The particles which carry color charge, i.e. the quarks, can interact via the strong force, the particles which carry electric charge, i.e. the quarks and charged leptons, can interact via the electromagnetic force, and all fundamental fermions can interact via the weak force. In addition, there is the Higgs boson which is responsible for the circumstance that the carriers of the weak interaction and the massive particles have mass (the photon and the gluons are massless in the SM).

It should also be pointed out that the three neutrinos are postulated to be massless in the SM. This is the case because a Dirac mass term would require right-handed Dirac neutrinos which are not observed experimentally. In order to obtain neutrino masses, it is necessary to extend the SM. This can be done by introducing right-handed sterile neutrinos, i.e. neutrinos which do not interact weakly, or by allowing neutrinos to be of Majorana type. In the framework of these extensions, the smallness of neutrino masses (compared to the masses of the charged leptons) can be motivated. This is done by means of the so called seesaw mechanism where very heavy right-handed neutrinos are responsible for the small masses of the left-handed neutrinos.

1.3 Neutrino oscillations

Neutrino oscillations are processes in which a neutrino, that was produced in one of the three flavor states ν_e , ν_μ , or ν_τ , travels a certain distance and does not necessarily retain its initial flavor state. This means that it is possible that the neutrino is found in one of the two other flavor states. The idea for these neutrino oscillations was firstly introduced by Bruno Pontecorvo [1, 2].

The neutrino-oscillation framework which coincides best with experimental results requires massive neutrinos. More specifically, it requires at least two massive neutrinos with different masses. In addition, the neutrino mass eigenstates (i.e. the states with definite mass) must not be the same as the neutrino flavor eigenstates, which means that there must be neutrino mixing. In other words, a neutrino flavor eigenstate is a linear combination of neutrino mass eigenstates. In the extreme relativistic limit, which is the normal case for propagating neutrinos, the probability for neutrino oscillations taking place is not dependent on the absolute neutrino masses but only on their mass squared differences $\Delta m_{ij}^2 = m_i^2 - m_j^2$, where m_i is the mass of the neutrino mass eigenstate $|\nu_i\rangle$. This is the standard neutrino-oscillation case and therefore, these oscillations are

called standard mass-difference neutrino oscillations. Their mechanism will be further discussed in Chapter 2.

1.4 Outlook

This thesis is concerned with the oscillation of high-energy cosmogenic neutrinos and antineutrinos, i.e. neutrinos and antineutrinos which have travelled very long distances before arriving on Earth. The creation of high-energy cosmogenic neutrinos and antineutrinos is related to ultrahigh-energy cosmic rays, which will be discussed in Chapter 3. High-energy cosmogenic neutrinos and antineutrinos are produced in scattering processes of ultrahigh-energy cosmic rays and cosmic backgrounds at microwave, infrared, optical, and ultraviolet wavelengths. The most important process is the scattering off the cosmic microwave background, known as the Greisen–Zatsepin–Kuzmin mechanism. The Greisen–Zatsepin–Kuzmin mechanism forms, along with the corresponding scattering processes involving the other cosmic backgrounds, the dominant source of cosmogenic neutrinos and antineutrinos in the energy range between 10^{14} eV and 10^{20} eV.

An experiment sensitive to high-energy cosmogenic neutrinos and antineutrinos is the IceCube neutrino observatory, which will be discussed in Chapter 4. It is sensitive to high-energy tau neutrinos and antineutrinos via several different tau neutrino/antineutrinos induced signatures. The energy of these cosmogenic tau neutrinos and antineutrinos is much higher than the neutrino energies available at other present neutrino-oscillation experiments. Therefore, it can serve as an instrument to probe neutrino oscillations for nonstandard contributions, since standard mass-difference neutrino oscillations are more and more suppressed with increasing neutrino energy. In this thesis, the focus is put on the case of nonstandard contributions arising from Fermi-point splitting. It is assumed that neutrinos have Fermi-point splitting, analogous to the occurrence of Fermi-point splitting in quantum phase transitions of fermionic atomic gases at ultralow temperatures. The effect of Fermi-point splitting on neutrino oscillations compared to the standard mass-difference case (Chapter 5) and the resulting implications for the results of the IceCube experiment will be discussed in Chapter 6. In particular, it will be analyzed up to which order of magnitude the IceCube experiment is sensitive to contributions from Fermi-point splitting and what impact the case of possible CP violation in the Fermi-point splitting sector can have.

Chapter 2

Standard mass-difference neutrino oscillations

The principle of standard mass-difference (MD) neutrino oscillations is relatively simple and equals that of many other quantum mechanical systems. If we consider, for example, a quantum system with two energy levels E_1 and E_2 , then the eigenstates of the system are the states which diagonalize its Hamiltonian. Note that if the system is in an initial state which does not correspond to one of the eigenstates, then the probability to find the system in this state oscillates in time with a frequency $\omega_{21} = E_2 - E_1$.

In standard MD neutrino oscillations, the neutrino mass matrix takes the role of the Hamiltonian. The mass matrix is diagonal in the basis of the neutrino mass eigenstates, but in general, the flavor eigenstates are not the same as the mass eigenstates. Thus, for a neutrino created in a specific flavor state, the probability to find the neutrino in this very state oscillates with time.

If we consider standard MD neutrino oscillations in the case of a Dirac neutrino mass term, the part of the Lagrangian which describes the lepton masses and charged current weak interactions is given by

$$\mathcal{L}_\ell = -\frac{g}{\sqrt{2}} \overline{\ell_{\alpha L}} \gamma^\mu \nu_{\alpha L} W_\mu^\dagger - \overline{\ell_{\alpha L}} (M_\ell)_{\alpha\beta} \ell_{\beta R} - \overline{\nu_{\alpha L}} (M_\nu)_{\alpha\beta} \nu_{\beta R} + h.c., \quad (2.1)$$

where g is a coupling constant, ℓ_α denotes the charged lepton flavor eigenfields, ν_α the neutrino flavor eigenfields, W_μ is one of the weak gauge fields, M_ℓ the charged lepton mass matrix, and M_ν the neutrino mass matrix.

The matrices M_ℓ and M_ν are complex matrices which can be diagonalized by bi-unitary transformations. We can choose unitary matrices U_L , U_R , V_L , and V_R such that

$$U_L^\dagger \cdot M_\nu \cdot U_R = \mathcal{M}_\nu, \quad (2.2a)$$

$$V_L^\dagger \cdot M_\ell \cdot V_R = \mathcal{M}_\ell, \quad (2.2b)$$

where \mathcal{M}_ν and \mathcal{M}_ℓ are diagonal matrices. Then, we can define the neutrino and charged lepton mass eigenfields to be¹

$$\nu_{iL} = (U_L^\dagger)_{i\alpha} \nu_{\alpha L}, \quad (2.3a)$$

$$\nu_{iR} = (U_R^\dagger)_{i\alpha} \nu_{\alpha R}, \quad (2.3b)$$

$$\ell_{iL} = (V_L^\dagger)_{i\alpha} \ell_{\alpha L}, \quad (2.3c)$$

$$\ell_{iR} = (V_R^\dagger)_{i\alpha} \ell_{\alpha R}. \quad (2.3d)$$

Now, the Lagrangian in Eq. (2.1) can be written in the mass eigenfield basis as

$$\mathcal{L}_\ell = -\frac{g}{\sqrt{2}} \overline{\ell_{iL}} \gamma^\mu U_{ij} \nu_{jL} W_\mu^\dagger - \overline{\ell_{iL}} m_{\ell i} \ell_{iR} - \overline{\nu_{iL}} m_{\nu i} \nu_{iR} + h.c., \quad (2.4)$$

where $m_{\ell i} = (\mathcal{M}_\ell)_{ii}$ are the charged lepton masses and $m_{\nu i} = (\mathcal{M}_\nu)_{ii}$ are the neutrino masses. The matrix $U = V_L^\dagger U_L$ is called the leptonic mixing matrix or the Maki–Nakagawa–Sakata (MNS) matrix [3] which is the leptonic analog of the Cabibbo–Kobayashi–Maskawa (CKM) matrix in the quark sector.

2.1 General neutrino-oscillation probability

The leptonic mixing matrix relates the neutrino flavor eigenstates $|\nu_\alpha\rangle$ to the neutrino mass eigenstates $|\nu_i\rangle$:

$$|\nu_\alpha\rangle = U_{\alpha i}^* |\nu_i\rangle. \quad (2.5)$$

If a neutrino is created in the initial flavor state $|\nu_\alpha\rangle$ at time $t = 0$, we can now calculate the probability of finding the neutrino at a later time t in the flavor state $|\nu_\beta\rangle$. For doing this, it is convenient to calculate the time evolution of the initial state in the mass eigenstate basis, since the neutrino mass matrix expressed in this basis is diagonal and therefore, the time evolution of an initial state is given by just multiplying a phase factor. In the mass eigenstate basis, the initial state at $t = 0$ becomes $|\nu(0)\rangle \equiv |\nu_\alpha\rangle = U_{\alpha i}^* |\nu_i\rangle$. The neutrino state at later time t is then

$$|\nu(t)\rangle = \sum_j U_{\alpha j}^* \exp(-iE_j t) |\nu_j\rangle, \quad (2.6)$$

¹Latin indices denote mass eigenfields, whereas Greek indices denote flavor eigenfields. It is summed over double indices.

where the E_j are the energy eigenvalues of the mass eigenstates. The probability amplitude that the neutrino is in the flavor eigenstate $|\nu_\beta\rangle$ at time t becomes

$$\begin{aligned} A^{\text{MD}}(\nu_\alpha \rightarrow \nu_\beta; t) &= \langle \nu_\beta | \nu(t) \rangle = \sum_j U_{\alpha j}^* \exp(-iE_j t) \langle \nu_\beta | \nu_j \rangle \\ &= \sum_j U_{\beta k} U_{\alpha j}^* \exp(-iE_j t) \langle \nu_k | \nu_j \rangle = \sum_j U_{\beta k} U_{\alpha j}^* \exp(-iE_j t) \delta_{kj} \\ &= \sum_j U_{\beta j} \exp(-iE_j t) U_{\alpha j}^* = \sum_j U_{\beta j} \exp(-iE_j t) U_{j\alpha}^\dagger. \end{aligned} \quad (2.7)$$

The physical meaning of the final expression is that $U_{j\alpha}^\dagger$ transforms the initial flavor eigenstate $|\nu_\alpha\rangle$ into the mass eigenstate $|\nu_j\rangle$. The factor $\exp(-iE_j t)$ is the propagator describing the time evolution in the mass eigenstate basis and $U_{\beta j}$ transforms the time-evolved mass eigenstate $|\nu_j\rangle$ back into the flavor basis, namely into the flavor eigenstate $|\nu_\beta\rangle$. The probability for an oscillation between two flavor eigenstates, i.e. the probability of a transition between these two states is then

$$P^{\text{MD}}(\nu_\alpha \rightarrow \nu_\beta; t) = |A^{\text{MD}}(\nu_\alpha \rightarrow \nu_\beta; t)|^2 = \left| \sum_j U_{\beta j} \exp(-iE_j t) U_{j\alpha}^\dagger \right|^2. \quad (2.8)$$

This is the general form of the MD neutrino-oscillation probability for an arbitrary number of flavors.

2.2 Two-flavor case

A simple case of standard MD neutrino oscillations is the two-flavor case, i.e. we assume to have only two neutrino flavors ν_e and ν_μ . In this case, the leptonic mixing matrix U can be written as

$$U \equiv U(\theta_0) = \begin{pmatrix} \cos(\theta_0) & \sin(\theta_0) \\ -\sin(\theta_0) & \cos(\theta_0) \end{pmatrix}, \quad (2.9)$$

where θ_0 is the neutrino mixing angle with the domain

$$\theta_0 \in \left[0, \frac{\pi}{4}\right]. \quad (2.10)$$

Then, the relation between the neutrino flavor and mass eigenstates is as follows

$$\begin{aligned} |\nu_e\rangle &= \cos(\theta_0) |\nu_1\rangle + \sin(\theta_0) |\nu_2\rangle, \\ |\nu_\mu\rangle &= -\sin(\theta_0) |\nu_1\rangle + \cos(\theta_0) |\nu_2\rangle. \end{aligned} \quad (2.11)$$

If we substitute Eq. (2.11) into the general MD neutrino-oscillation probability (2.8), we obtain

$$P^{\text{MD}}(\nu_e \rightarrow \nu_\mu; t) = P^{\text{MD}}(\nu_\mu \rightarrow \nu_e; t) = \sin^2(2\theta_0) \sin^2 \left[\frac{1}{2}(E_2 - E_1)t \right]. \quad (2.12)$$

If we further take into account that for relativistic neutrinos with momentum p , kinetic energy E_ν , and masses m_j ,

$$E_j = \sqrt{p^2 + m_j^2} \simeq p + \frac{m_j^2}{2p} \simeq p + \frac{m_j^2}{2E_\nu}, \quad (2.13)$$

Eq. (2.12) becomes

$$P^{\text{MD}}(\nu_e \rightarrow \nu_\mu; t) = P^{\text{MD}}(\nu_\mu \rightarrow \nu_e; t) = \sin^2(2\theta_0) \sin^2\left(\frac{\Delta m^2}{4E_\nu}t\right), \quad (2.14)$$

where $\Delta m^2 \equiv m_2^2 - m_1^2$.

The survival probabilities become

$$P^{\text{MD}}(\nu_e \rightarrow \nu_e; t) = P^{\text{MD}}(\nu_\mu \rightarrow \nu_\mu; t) = 1 - \sin^2(2\theta_0) \sin^2\left(\frac{\Delta m^2}{4E_\nu}t\right), \quad (2.15)$$

due to the condition

$$P^{\text{MD}}(\nu_\alpha \rightarrow \nu_e; t) + P^{\text{MD}}(\nu_\alpha \rightarrow \nu_\mu; t) = 1, \quad (2.16)$$

where $\alpha \in \{e, \mu\}$.

For relativistic neutrinos, it also holds that $L \simeq t$, with L being the distance travelled by the neutrinos. Using this fact, Eq. (2.14) can be written as

$$P^{\text{MD}}(\nu_e \rightarrow \nu_\mu; L) = P^{\text{MD}}(\nu_\mu \rightarrow \nu_e; L) = \sin^2(2\theta_0) \sin^2\left(1.27 \Delta m^2 \frac{L}{E_\nu}\right), \quad (2.17)$$

where L is in m and E_ν in MeV or L is in km and E_ν in GeV.

We observe that the MD neutrino-oscillation probability consists of two factors. An amplitude which is only dependent on the mixing angle θ_0 and an oscillation factor which depends on the neutrino mass squared difference, the neutrino energy E_ν , and the distance L travelled by the neutrinos. In neutrino experiments, the distance L , i.e. the baseline of the experiment, is normally kept fixed and the energy E_ν is the the only variable. In order to obtain a sufficiently large neutrino-oscillation probability in the energy range of an experiment (which has a lower limit) the oscillation phase must not be too small, i.e. the baseline must be long enough. On the other hand, the detectors in neutrino experiments have limited energy resolution. Therefore, neutrino oscillations must not be too fast in order to observe the oscillatory behavior and not just the constant average. This means that the oscillation phase must not be too large and the same has to hold for the baseline.

2.3 Three-flavor case

In the case of three neutrino flavors (ν_e , ν_μ , and ν_τ), the leptonic mixing matrix U depends on three mixing angles θ_{12} , θ_{13} , and θ_{23} and one (CP violating²) phase δ . The

²This will be further discussed in Sec. 2.4.

standard parameterization coincides with the standard parameterization of the quark mixing matrix:

$$U(\theta_{12}, \theta_{13}, \theta_{23}, \delta) = \begin{pmatrix} c_{12} c_{13} & s_{12} c_{13} & s_{13} e^{-i\delta} \\ -s_{12} c_{23} - c_{12} s_{23} s_{13} e^{i\delta} & c_{12} c_{23} - s_{12} s_{23} s_{13} e^{i\delta} & s_{23} c_{13} \\ s_{12} s_{23} - c_{12} c_{23} s_{13} e^{i\delta} & -c_{12} s_{23} - s_{12} c_{23} s_{13} e^{i\delta} & c_{23} c_{13} \end{pmatrix}, \quad (2.18)$$

where $s_{ij} \equiv \sin \theta_{ij}$ and $c_{ij} \equiv \cos \theta_{ij}$. The domains of the mixing angles θ_{ij} and the phase δ are [4]

$$\theta_{ij} \in \left[0, \frac{\pi}{2}\right], \quad (2.19a)$$

$$\delta \in [0, 2\pi]. \quad (2.19b)$$

It is instructive to define the evolution Hamiltonian H'_{MD} expressed in flavor eigenstate basis

$$\begin{aligned} H'_{\text{MD}} &= U(\theta_{12}, \theta_{13}, \theta_{23}, \delta) \cdot \text{diag} (E_1, E_2, E_3) \cdot U^\dagger(\theta_{12}, \theta_{13}, \theta_{23}, \delta) \\ &\simeq U(\theta_{12}, \theta_{13}, \theta_{23}, \delta) \cdot \text{diag} \left(p + \frac{m_1^2}{2E_\nu}, p + \frac{m_2^2}{2E_\nu}, p + \frac{m_3^2}{2E_\nu} \right) \cdot U^\dagger(\theta_{12}, \theta_{13}, \theta_{23}, \delta), \end{aligned} \quad (2.20)$$

where condition (2.13) has been applied. Since terms proportional to the identity $\mathbf{1}$ only result in an overall phase factor, we can define a new evolution Hamiltonian H_{MD}

$$H_{\text{MD}} \equiv H'_{\text{MD}} - \left(p + \frac{m_1^2}{2E_\nu} \right) \mathbf{1}, \quad (2.21)$$

which does not alter the MD neutrino-oscillation probabilities. It has the explicit form

$$H_{\text{MD}} = \frac{1}{2E_\nu} U(\theta_{12}, \theta_{13}, \theta_{23}, \delta) \cdot \text{diag} (0, \Delta m_{21}^2, \Delta m_{31}^2) \cdot U^\dagger(\theta_{12}, \theta_{13}, \theta_{23}, \delta), \quad (2.22)$$

where $\Delta m_{k1}^2 \equiv m_k^2 - m_1^2$.

Contrary to the two-flavor case, the MD neutrino-oscillation probabilities with three flavors, which can be calculated by means of Eq. (2.8), do not have a simple form. However, we can apply some limiting cases which are of practical interest and lead to simple approximate expressions for the MD neutrino-oscillation probabilities in the framework of two-flavor MD neutrino oscillations. At first, one can assume a hierarchy between the mass squared differences

$$|\Delta m_{21}^2| \ll |\Delta m_{31}^2|, \quad (2.23)$$

which is based on the results of solar and atmospheric neutrino experiments. This hierarchy allows two cases: either $m_1 \ll m_2 \ll m_3$ which is called normal hierarchy or $m_3 \ll m_1 \leq m_2$ which is called inverted hierarchy.

Consider now the limiting case $\Delta m_{21}^2 \rightarrow 0$. This case is of interest in atmospheric, reactor, and accelerator neutrino experiments. The probability for oscillations between two neutrino flavor states then takes the form

$$P^{\text{MD}}(\nu_\alpha \rightarrow \nu_\beta; L) = 4 |U_{\alpha 3}|^2 |U_{\beta 3}|^2 \sin^2 \left(\frac{\Delta m_{31}^2 L}{4E_\nu} \right). \quad (2.24)$$

This has the same form as the MD neutrino-oscillation probability in the two-flavor case. The MD neutrino-oscillation probabilities among ν_e , ν_μ , and ν_τ then are as follows

$$\begin{aligned} P^{\text{MD}}(\nu_e \rightarrow \nu_\mu; L) &= 4 |U_{e3}|^2 |U_{\mu 3}|^2 \sin^2 \left(\frac{\Delta m_{31}^2 L}{4E_\nu} \right) \\ &= \sin^2(\theta_{23}) \sin^2(2\theta_{13}) \sin^2 \left(\frac{\Delta m_{31}^2 L}{4E_\nu} \right), \end{aligned} \quad (2.25)$$

$$\begin{aligned} P^{\text{MD}}(\nu_e \rightarrow \nu_\tau; L) &= 4 |U_{e3}|^2 |U_{\tau 3}|^2 \sin^2 \left(\frac{\Delta m_{31}^2 L}{4E_\nu} \right) \\ &= \cos^2(\theta_{23}) \sin^2(2\theta_{13}) \sin^2 \left(\frac{\Delta m_{31}^2 L}{4E_\nu} \right), \end{aligned} \quad (2.26)$$

$$\begin{aligned} P^{\text{MD}}(\nu_\mu \rightarrow \nu_\tau; L) &= 4 |U_{\mu 3}|^2 |U_{\tau 3}|^2 \sin^2 \left(\frac{\Delta m_{31}^2 L}{4E_\nu} \right) \\ &= \cos^4(\theta_{13}) \sin^2(2\theta_{23}) \sin^2 \left(\frac{\Delta m_{31}^2 L}{4E_\nu} \right), \end{aligned} \quad (2.27)$$

with $P^{\text{MD}}(\nu_\beta \rightarrow \nu_\alpha) = P^{\text{MD}}(\nu_\alpha \rightarrow \nu_\beta)$.

Another limiting case is the one valid for solar MD neutrino oscillations and very long-baseline reactor experiments. For this case, it holds that

$$\frac{\Delta m_{31}^2 L}{2E_\nu} \gg 1. \quad (2.28)$$

Then, the neutrino oscillations due to the mass squared differences Δm_{31}^2 are fast and only cause an average effect. The electron neutrino survival probability becomes approximately

$$P^{\text{MD}}(\nu_e \rightarrow \nu_e) \simeq \cos^4(\theta_{13}) P + \sin^4(\theta_{13}), \quad (2.29)$$

where P is the ν_e survival probability in the two-flavor case with $\Delta m^2 = \Delta m_{21}^2$ and $\theta_0 = \theta_{12}$, i.e.

$$P = 1 - \sin^2(2\theta_{12}) \sin^2 \left(\frac{\Delta m_{21}^2 L}{4E_\nu} \right). \quad (2.30)$$

2.4 CP, T, and CPT invariances

Let us recall the equations for the general MD neutrino-oscillation amplitude, Eq. (2.7)

$$A^{\text{MD}}(\nu_\alpha \rightarrow \nu_\beta; t) = \sum_j U_{\beta j} \exp(-iE_j t) U_{\alpha j}^*, \quad (2.31)$$

and for the general MD neutrino-oscillation probability, Eq. (2.8)

$$P^{\text{MD}}(\nu_\alpha \rightarrow \nu_\beta; t) = \left| \sum_j U_{\beta j} \exp(-iE_j t) U_{\alpha j}^* \right|^2. \quad (2.32)$$

In the case of neutrinos, CP essentially acts as the transformation between neutrinos and antineutrinos. This action corresponds to the transformation of the leptonic mixing matrix $U \rightarrow U^*$. If one has CP invariance, this means that the MD neutrino-oscillation probabilities between neutrinos and the corresponding antineutrinos coincide:

$$P^{\text{MD}}(\nu_\alpha \rightarrow \nu_\beta; t) = P^{\text{MD}}(\bar{\nu}_\alpha \rightarrow \bar{\nu}_\beta; t) \quad (2.33)$$

or

$$\left| \sum_j U_{\beta j} \exp(-iE_j t) U_{\alpha j}^* \right|^2 = \left| \sum_j U_{\beta j}^* \exp(-iE_j t) U_{\alpha j} \right|^2, \quad (2.34)$$

from which we can conclude that we need to have $U = U^*$ for CP invariance.

An interesting question now arising is when CP is not conserved. For n neutrino flavors, U is a general unitary $n \times n$ matrix and it can be parametrized by $n(n-1)/2$ angles and $n(n+1)/2$ phases. In the case of Dirac neutrinos, $2n-1$ phases can be absorbed into the left-handed fields and therefore, $(n-1)(n-2)/2$ physical phases remain. From this follows that the condition $U = U^*$ and CP conservation can only be violated for $n \geq 3$ neutrino flavors.

If we look at T transformations, these have the action $t \rightarrow -t$. For the MD neutrino-oscillation amplitude (2.31), this means that

$$\begin{aligned} A^{\text{MD}}(\nu_\alpha \rightarrow \nu_\beta; t) &= \sum_j U_{\beta j} \exp(-iE_j t) U_{\alpha j}^* \xrightarrow{\text{T}} \\ A^{\text{MD}}(\nu_\alpha \rightarrow \nu_\beta; -t) &= \sum_j U_{\beta j} \exp(+iE_j t) U_{\alpha j}^* = \left(\sum_j U_{\alpha j} \exp(-iE_j t) U_{\beta j}^* \right)^* \\ &= (A^{\text{MD}}(\nu_\beta \rightarrow \nu_\alpha; t))^*, \end{aligned} \quad (2.35)$$

and therefore, it follows for the oscillation probability (2.32)

$$P^{\text{MD}}(\nu_\alpha \rightarrow \nu_\beta; t) \xrightarrow{\text{T}} P^{\text{MD}}(\nu_\alpha \rightarrow \nu_\beta; -t) = P^{\text{MD}}(\nu_\beta \rightarrow \nu_\alpha; t), \quad (2.36)$$

which means that T interchanges the initial and final neutrino state. For T invariance we then have

$$P^{\text{MD}}(\nu_\alpha \rightarrow \nu_\beta; t) = P^{\text{MD}}(\nu_\beta \rightarrow \nu_\alpha; t) \quad (2.37)$$

or

$$\left| \sum_j U_{\beta j} \exp(-iE_j t) U_{\alpha j}^* \right|^2 = \left| \sum_j U_{\alpha j} \exp(-iE_j t) U_{\beta j}^* \right|^2. \quad (2.38)$$

However, this is nothing else but Eq. (2.34) which we had for CP invariance. Thus, for T being conserved we need as for CP conservation: $U = U^*$. This is not very surprising, since we expect CPT invariance and therefore, if CP is conserved, T must be conserved as well.

It remains to show that CPT is conserved. The combined application of the transformations $U \rightarrow U^*$ and $t \rightarrow -t$ has the following action on the MD neutrino-oscillation amplitude (2.31)

$$\begin{aligned} A^{\text{MD}}(\nu_\alpha \rightarrow \nu_\beta; t) &= \sum_j U_{\beta j} \exp(-iE_j t) U_{\alpha j}^* \xrightarrow{\text{CPT}} \\ A^{\text{MD}}(\bar{\nu}_\alpha \rightarrow \bar{\nu}_\beta; -t) &= \sum_j U_{\beta j}^* \exp(+iE_j t) U_{\alpha j} = (A^{\text{MD}}(\bar{\nu}_\beta \rightarrow \bar{\nu}_\alpha; t))^* \\ &= (A^{\text{MD}}(\nu_\alpha \rightarrow \nu_\beta; t))^*, \end{aligned} \quad (2.39)$$

which means that CPT turns the oscillation amplitude into its complex conjugate and we have indeed CPT invariance:

$$P^{\text{MD}}(\nu_\alpha \rightarrow \nu_\beta; t) = P^{\text{MD}}(\bar{\nu}_\beta \rightarrow \bar{\nu}_\alpha; t). \quad (2.40)$$

Chapter 3

Ultrahigh-energy cosmic rays and cosmogenic neutrinos

It is known that there exist ultrahigh-energy (UHE) cosmic rays with energies above 10^{18} eV and even exceeding 10^{20} eV. These UHE cosmic rays mainly consist of protons, but, in principle, also heavier elements, e.g. iron nuclei, are possible constituents. Ultrahigh-energy cosmic rays can scatter off cosmic microwave background (CMB) photons, a process which is called Greisen–Zatsepin–Kuzmin (GZK) mechanism [5, 6]. Furthermore, the same scattering can take place with photons of the cosmic ultraviolet-optical (CUVOB) and infrared (CIB) backgrounds [7]. Both processes are the main sources of cosmogenic neutrinos and antineutrinos with energies above 10^{14} eV.

In the following, a short introduction to UHE cosmic rays (Sec. 3.1) and the cosmic microwave, UV-optical, and infrared backgrounds (Sec. 3.2) will be given, followed by the description of the GZK mechanism in Sec. 3.3 and the cosmic ray scattering off the cosmic UV-optical and infrared backgrounds in Sec. 3.4. In Sec. 3.5, the content of the preceding sections will be used to determine the energy spectrum of high-energy cosmogenic neutrinos and antineutrinos.

3.1 Possible origin of ultrahigh-energy cosmic rays

The creation process of UHE cosmic rays is to a large extent unknown. However, there are a number of possible candidates for UHE cosmic ray sources like neutron stars, active galactic nuclei (AGNs), radio galaxies, or gamma ray bursts (GRBs).

A first estimate for UHE cosmic ray sources was already performed by Hillas in 1984 [8]. He connected the accelerating process of a cosmic ray particle with charge Ze to the Larmor radius r_L of a relativistic particle with energy E in a magnetic field with field strength B . The Larmor radius r_L is given by

$$r_L = 1.08 \frac{E}{ZB}, \quad (3.1)$$

where r_L is in parsec, B in microgauss, and E in units of 10^{15} eV. If the particles are gradually accelerated by making many irregular loops in the magnetic field and thereby gaining energy, the size L of the accelerating region with sufficiently strong B has to be much larger than two times the Larmor radius

$$L \gg 2r_L \sim 2 \frac{E}{ZB}. \quad (3.2)$$

More precisely, this can be described by the mechanism of Fermi acceleration. Then, the energy gain of the charged particles occurs by reflection from distinct magnetized “clouds” which move with velocity $v \equiv \beta c$. In this case, the mean acceleration time t_a can be expressed by

$$t_a = \frac{\lambda}{2c\beta^2}, \quad (3.3)$$

where λ is the mean free path between two scattering events of the charged particle. On the other hand, the mean escape time t_e for a charged particle leaving a sphere of radius R containing the magnetized clouds is

$$t_e \sim 1.5 \frac{R^2}{c\lambda}. \quad (3.4)$$

If we assume

$$\lambda \sim r_L, \quad (3.5)$$

and additionally demand

$$t_e > t_a, \quad (3.6)$$

it follows that

$$L \equiv 2R \gtrsim \frac{r_L}{\beta} \sim \frac{E}{ZB\beta}, \quad (3.7)$$

where L is in parsec, B in microgauss, and E in units of 10^{15} eV, as in Eq. (3.1).

Condition (3.7) for protons and iron nuclei is shown in Fig. 3.1 along with possible sites of cosmic ray acceleration. It is apparent that only few candidates can be considered to be able to accelerate charged particles to energies of 10^{20} eV. A few of these candidates will be described in the following.

3.1.1 Neutron stars

A neutron star is the remnant of a massive star, more precisely of the core of the star. As the name suggests it consists mainly of neutrons.

When a massive star explodes in a supernova at the end of its life time, its core is compressed and finally collapses into a neutron star, the diameter L of which is of the order of several kilometers. In this process, the neutron star retains most of the star core’s angular momentum, but it has only a fraction of the size of the original core.

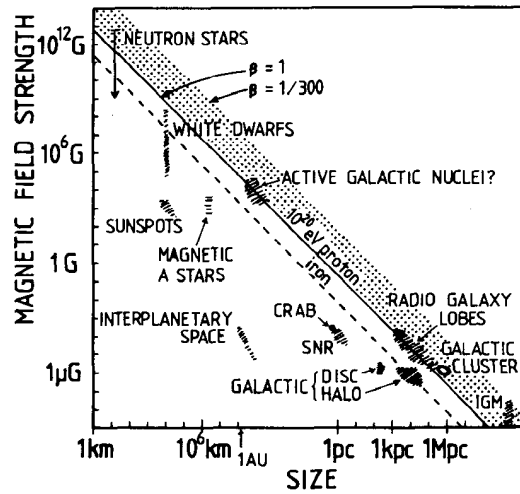


Figure 3.1. Size L and magnetic field strength B of possible sites of cosmic ray acceleration, as given in [8]. Objects below the solid/dashed diagonal line are not able to accelerate protons/iron nuclei to energies of 10^{20} eV. β is the velocity of scattering centers in the Fermi acceleration process divided by the speed of light, as discussed in the main text.

Thus, a neutron star can have very high rotation velocities with rotation periods of the order of milliseconds. Additionally, the product of star cross-section and the magnetic field strength on the star surface is conserved due to energy conservation which leads to very high magnetic field strengths B on the surface of a neutron star of the order of 10^{12} G. The magnetosphere of a neutron star co-rotates with the star itself leading to a high velocity β of scattering centers in the Fermi acceleration process. The combination of small size L , high magnetic field strength B , and high velocity β makes neutron stars suitable candidates for sources of UHE cosmic rays.

3.1.2 Active galactic nuclei and radio galaxies

It is believed that in the center of all massive galaxies, there exist supermassive black holes (with masses between 10^6 and 10^{10} times that of the Sun). The high gravitational force of these black holes forces the surrounding galactic matter to form a so called accretion disc, from which the matter spirals into the black hole. Inside the accretion disc, high temperatures prevail, which makes it an optically very active region. This central active region with the black hole and the accretion disc forms the AGN.

In many cases a central AGN powers two large lobes of a radio galaxy. These lobes are very active in the radio wave band due to synchrotron radiation losses inside the lobes. This is a result of the relativistic velocity of matter inside the lobe of the order $\beta \sim 0.3$.

Ultrahigh-energy cosmic rays can be produced inside AGNs as well as in radio galaxy lobes. An AGN has an extension $L \sim 0.1$ pc with magnetic field strengths $B \sim 1$ G. A radio galaxy lobe is much larger than the central AGN, with an extension L of the order of 10 kpc. On the other hand, the magnetic field strength B inside the lobe is much weaker and of the order of $100 \mu\text{G}$.

3.1.3 Gamma ray bursts

Gamma ray bursts are flashes of high-energy radiation that can be brighter than any other gamma ray source in the sky. They can occur as single-peaked bursts, but also as bursts with fast rising and exponential decaying gamma ray flux or the inverse of the latter. The duration of GRBs is typically a few seconds, but can range from a few milliseconds to minutes.

The collapsar model is the currently favored model for the creation process of most observed GRBs. When the core of an extremely massive, rapidly-rotating star collapses into a black hole, the infall of material from the star onto the black hole powers two extremely energetic jets of relativistically expanding plasma consisting of photons, electrons, and positrons. The optical depth in the initial plasma jet is high enough that the photons have energies above the pair production threshold. With progressing expansion of the jets, the optical depth is reduced and the photon energy falls below the pair production threshold. This allows the photons to exit the plasma and the GRB is created.

The fast moving plasma of the jets also creates high magnetic field strengths B and leads to high velocity β of scattering centers in Fermi acceleration. Together with a dimension L of the GRB jets of the order of 10^{-5} pc, these jets form a possible source for UHE cosmic rays.

A presently running experiment measuring the spectrum of UHE cosmic rays is the Pierre Auger Observatory [9]. The spectrum which this experiment observed is given in Fig. 3.2. It shows that the spectrum of UHE cosmic rays J follows a power law in cosmic ray energy E

$$J \propto E^{-2.6}, \quad (3.8)$$

for $E \lesssim 10^{19.6}$ eV. Above this energy, a cutoff in the spectrum is observed. One explanation for this cutoff is the GZK mechanism which will be discussed in Sec. 3.3.

There are two other interesting results from the Pierre Auger Observatory. The first is that cosmic rays with energies above 5.6×10^{19} eV from sources closer than 75 Mpc^1 seem to be correlated with AGNs. The second is that the observed UHE cosmic rays

¹Cosmic rays with these high energies can only originate from close astrophysical sources (up to a distance of the order of 100 Mpc) due to the GZK mechanism.

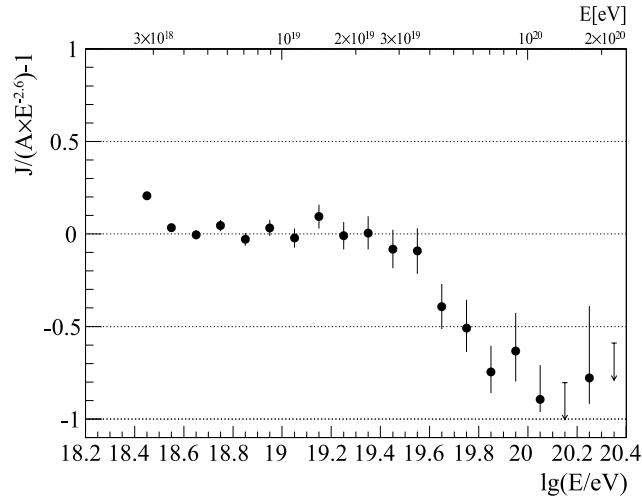


Figure 3.2. Ratio of the UHE cosmic ray spectrum J measured by the Pierre Auger Observatory and a power law behavior $\propto E^{-2.6}$ as a function of cosmic ray energy E [9].

are most likely protons. Particles with greater charge, e.g. iron nuclei, would undergo a deflection in the magnetic field of our galaxy which is too strong for being compatible with the measured anisotropic distribution of UHE cosmic rays [10].

3.2 Cosmic microwave, ultraviolet-optical, and infrared backgrounds

The most known cosmic background radiation is the cosmic microwave background radiation (CMBR). It corresponds to the radiation of a black body with a temperature of 2.7 K and is considered as evidence for the inflationary big bang theory, which involves the expansion of the universe after the initial big bang.

The present picture of the origin of the CMBR is as follows. During the first period of its existence the universe was in thermal equilibrium and photons were continually absorbed and emitted leading to a black body spectrum of the radiation. With proceeding expansion, the universe cooled down to a temperature of approximately 3000 K at which electrons and nuclei started to form hydrogen atoms, a process known as recombination. The recombination process stopped the main interaction mechanism between photons and matter, namely Thomson scattering, and the universe became transparent for photons. Thus, the photon field decoupled from matter, but retained its black body spectrum. This is the CMBR we observe today, but as a consequence of

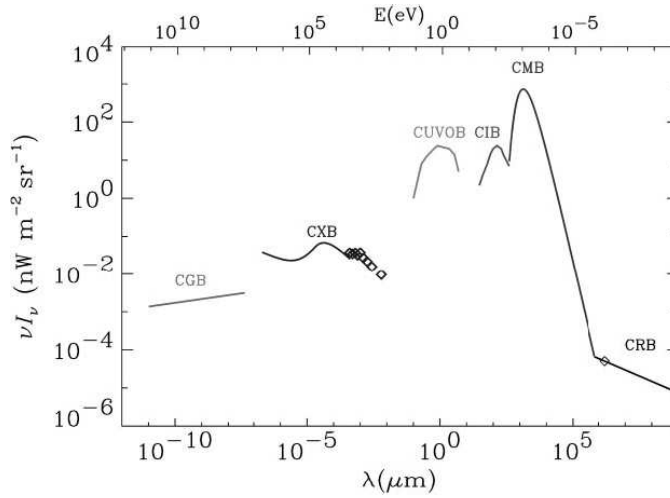


Figure 3.3. Spectrum of the cosmic background radiations as a function of photon energy E and wavelength λ , as given in [11]. Along with the CMB, the CIB, and the CUVOB, the cosmic radio background (CRB), the cosmic X-ray background (CXB), and the cosmic gamma ray background (CGB) are shown.

the subsequent expansion of the universe after the decoupling process, it is strongly redshifted compared to the radiation directly after decoupling. Therefore, the temperature of the CMBR today is 2.7 K which lies in the microwave region of the electromagnetic spectrum.

Besides the CMB, there are other cosmic backgrounds in different spectral areas. The CIB and the CUVOB are examples for these additional backgrounds. They do not follow a black body spectrum in contrast to the CMB, since they are the consequence of the electromagnetic radiation of galaxies. The superposition of the light of many galaxies with different distances to Earth, i.e. their light arrives with different redshifts on Earth, form these additional cosmic backgrounds.

Figure 3.3 shows the spectrum of the CMB, the CIB, and the CUVOB along with other cosmic backgrounds. The CMB follows the typical black body spectrum. Compared to the CMB, the CIB and the CUVOB are fainter, approximately two orders of magnitude, and all other backgrounds are at least four orders of magnitude below the CMB.

3.3 Greisen–Zatsepin–Kuzmin mechanism

Cosmic ray protons with extremely high energies can scatter off CMB photons. This process is known as the Greisen–Zatsepin–Kuzmin mechanism [5,6]. In this interaction,

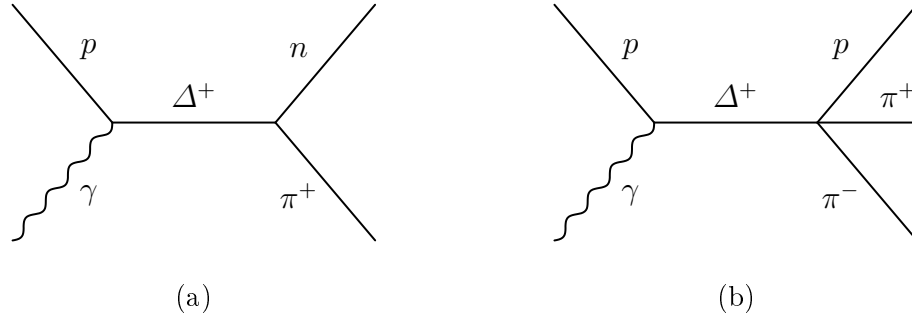


Figure 3.4. Feynman diagrams of the photopion processes (3.9a) represented by diagram (a) and (3.9b) represented by diagram (b). The diagrams were created with FeynArts [12].

the proton and the CMB photon create a Δ^+ resonance which subsequently decays into so called photopions. Examples for these reactions are

$$p + \gamma \longrightarrow \Delta^+ \longrightarrow n + \pi^+, \quad (3.9a)$$

$$p + \gamma \longrightarrow \Delta^+ \longrightarrow p + \pi^+ + \pi^-, \quad (3.9b)$$

the corresponding Feynman diagrams are given in Fig. 3.4. The proton energy E_p for these processes depending on the Δ^+ mass m_{Δ^+} , the proton mass m_p , the CMB photon energy E_γ , and the angle between the momenta of the initial proton and CMB photon θ is given by

$$E_p = \frac{m_{\Delta^+}^2 - m_p^2}{2E_\gamma(1 - \cos\theta)}. \quad (3.10)$$

The derivation of this formula can be found in Appendix A. For the reaction (3.9a), the effective proton threshold energy E_{GZK} can be calculated to be

$$E_{\text{GZK}} \simeq 8 \times 10^{19} \text{ eV}, \quad (3.11)$$

with $\theta = \pi$, $E_\gamma = 2 \times 10^{-3} \text{ eV}$, at which the photon energy density is 1/10 of its maximum, and the mass of the lightest Δ^+ , $m_{\Delta^+} = 1232 \text{ MeV}$ [13]. This has two consequences. First, we expect a cutoff in the cosmic-ray energy spectrum above E_{GZK} , the so called GZK cutoff [5,6]², since the cosmic-ray protons loose energy via reactions like (3.9a) and (3.9b) as long as their energy is above E_{GZK} . Second, the produced pions

²Experimental indication for the GZK cutoff is given in Sec. 3.1.

decay with neutrinos and antineutrinos as decay products [14], mainly in the following reactions (99.99 % branching ratio [13])

$$\pi^+ \longrightarrow \mu^+ + \nu_\mu \longrightarrow e^+ + \nu_e + \nu_\mu + \bar{\nu}_\mu, \quad (3.12a)$$

$$\pi^- \longrightarrow \mu^- + \bar{\nu}_\mu \longrightarrow e^- + \bar{\nu}_e + \bar{\nu}_\mu + \nu_\mu. \quad (3.12b)$$

These are the dominating GZK neutrino production processes for neutrino energies E_ν larger than $\sim 10^{17}$ eV. At lower energies, neutrons produced for examples in reactions like (3.9a) are the dominating source of GZK neutrinos. The neutrons almost completely undergo beta decay [13]

$$n \longrightarrow p + e^- + \bar{\nu}_e, \quad (3.13)$$

which results in the creation of electron antineutrinos. This is the dominating GZK neutrino production process for neutrino energies E_ν lower than $\sim 10^{17}$ eV.

3.4 Cosmic ray scattering off the cosmic UV-optical and infrared backgrounds

Besides the GZK mechanism, there is another very similar process, namely the interaction of cosmic ray protons with the infrared, optical, and ultraviolet photon background [7]. The difference is that photons of the CIB and CUVOB have energies E_γ which are up to three orders of magnitude larger than those of CMB photons. Thus, the threshold energy E_{UV} for cosmic ray protons undergoing these scattering process, which is defined by Eq. (3.10), is approximately three orders of magnitude lower than E_{GZK}

$$E_{UV} \simeq 10^{17} \text{ eV}. \quad (3.14)$$

However, the neutrino creation mechanisms (3.12a), (3.12b), and (3.13) stay the same.

The energy density of the CIB and the CUVOB is approximately two orders of magnitude lower than the energy density of the CMB. This greatly increases the mean free path for cosmic ray protons to undergo reactions like (3.9a) or (3.9b) compared to the corresponding mean free path in the GZK process. However, since the cosmic ray spectrum follows a power law, the flux of cosmic ray protons in the energy regime relevant to CIB and CUVOB scattering is almost eight orders of magnitude higher than that relevant to CMB scattering. This is why the flux of cosmogenic neutrinos and antineutrinos created as a result of CIB and CUVOB scattering is expected to be larger than that of GZK neutrinos and antineutrinos, but centered at a neutrino energy E_ν approximately three orders of magnitude lower than the GZK neutrino flux.³

³The combination of larger mean free path of cosmic ray protons and higher cosmic ray flux is also the reason why the cosmic ray spectrum is not significantly altered by CIB and CUVOB scattering in contrast to the GZK process which leads to the GZK cutoff.

3.5 Energy spectrum of high-energy cosmogenic neutrinos

Summarizing the two previous sections, high-energy cosmogenic neutrinos and antineutrinos are produced by pion decay in the ratio

$$N(\nu_e + \bar{\nu}_e) : N(\nu_\mu + \bar{\nu}_\mu) : N(\nu_\tau + \bar{\nu}_\tau) = 1 : 2 : 0, \quad (3.15)$$

where $N(\nu_\alpha + \bar{\nu}_\alpha)$ denotes the number of neutrinos and antineutrinos with flavor α . Moreover, they are created by neutron decay in the ratio

$$N(\nu_e + \bar{\nu}_e) : N(\nu_\mu + \bar{\nu}_\mu) : N(\nu_\tau + \bar{\nu}_\tau) = 1 : 0 : 0, \quad (3.16)$$

where the maximum of the neutrino spectrum of the latter process lies approximately two orders of magnitude below that of the former process. On the other hand, the spectrum of neutrinos and antineutrinos produced in CIB and CUVOB scattering is shifted approximately three orders of magnitude to lower energies compared to the spectrum of GZK neutrinos and antineutrinos. Since the spectral flux of neutrinos and antineutrinos produced in CIB and CUVOB scattering is larger than that of GZK neutrinos and antineutrinos, its pion decay component should dominate the neutron decay component of the GZK neutrino spectrum, i.e. we expect high-energy cosmogenic neutrinos and antineutrinos above a certain energy in the ratio

$$N(\nu_e + \bar{\nu}_e) : N(\nu_\mu + \bar{\nu}_\mu) : N(\nu_\tau + \bar{\nu}_\tau) = 1 : 2 : 0. \quad (3.17)$$

A quantitative calculation of the spectrum of high-energy cosmogenic neutrinos and antineutrinos including the described neutrino production processes was performed in Ref. [7]. Their result is shown in Fig. 3.5. In this work, however, we are not interested in the exact shape of the neutrino spectrum. We are only interested in the ratios of different neutrino flavors. Figure 3.5 shows that cosmogenic neutrinos and antineutrinos with energies above 10^{14} eV are to a very good degree generated in the ratio

$$N(\nu_e + \bar{\nu}_e) : N(\nu_\mu + \bar{\nu}_\mu) : N(\nu_\tau + \bar{\nu}_\tau) = 1 : 2 : 0, \quad (3.18)$$

as it was anticipated in the preceding considerations.

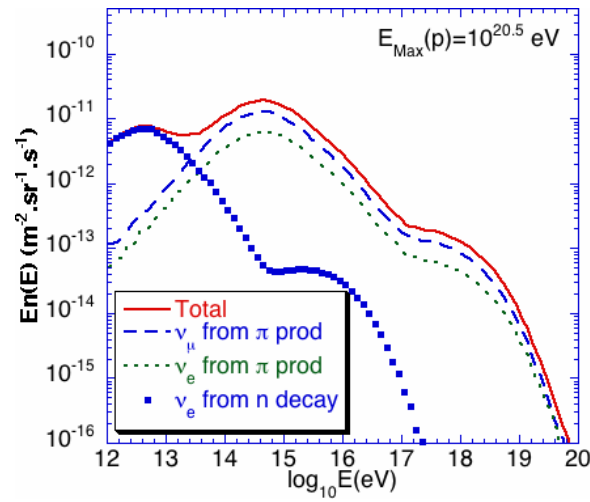


Figure 3.5. Estimated flux of cosmogenic neutrinos and antineutrinos dependent on neutrino energy E_ν , as given in [7]. The long-dashed line shows the combined flux of muon neutrinos and antineutrinos from photopion decay, the short-dashed line the combined flux of electron neutrinos and antineutrinos from photopion decay, the full squares the electron antineutrino flux from neutron decay, and the solid line corresponds to the sum of all contributions to the neutrino and antineutrino flux.

Chapter 4

IceCube experiment

The IceCube Neutrino Observatory [15] is a neutrino telescope located at the Amundsen-Scott base at the South Pole, Antarctica. It is the successor of the AMANDA telescope and will be the first km^3 sized neutrino detector.

The main neutrino detector material of IceCube is the polar ice at the South Pole. After completion, the detector will consist of an in-ice array situated in depths between 1450 m and 2450 m and it will cover an ice volume of about one km^3 . In detail, 80 strings with 60 digital optical modules (DOMs) each will be deployed in the ice in a hexagonal arrangement, with the strings being separated 125 m from each other. The DOMs are equipped with 25 cm diameter Hamamatsu photomultiplier tubes (PMTs) and electronics which digitize the measured signals. Additionally, the IceCube experiment features the IceTop air shower array at the surface. It will consist of two ice Cherenkov tanks close to the hole of each in-ice string and every tank will be equipped with two of the same DOMs which are in operation in the underground detector. The IceTop array will be used for calibration and background studies as well as a supplement to the in-ice detector in studying cosmic rays. Figure 4.1 shows a graphical representation of the IceCube experiment with the in-ice strings and the IceTop air shower array.

At the beginning of 2007, 22 in-ice strings and 26 IceTop stations were deployed [16] and it is planned to install 14 additional strings and IceTop stations every austral summer.

4.1 Tau neutrino events in the IceCube experiment

In Chapter 5, it will be discussed in detail that standard MD neutrino oscillations lead to the following ratio of cosmogenic neutrinos and antineutrinos with energy $E_\nu > 10^{14}$ eV on Earth:

$$N(\nu_e + \bar{\nu}_e) : N(\nu_\mu + \bar{\nu}_\mu) : N(\nu_\tau + \bar{\nu}_\tau) = 1 : 1 : 1. \quad (4.1)$$

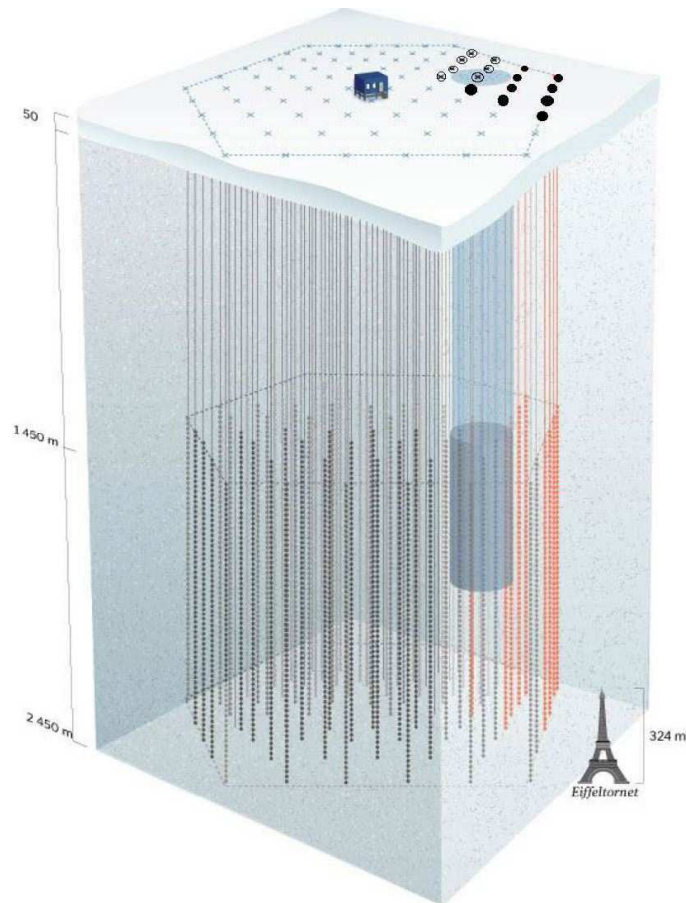


Figure 4.1. The IceCube neutrino observatory with the IceTop air shower array at the surface and in-ice strings. For illustration, a true-to-scale image of the Eiffel tower is included. The AMANDA telescope is included in IceCube and is indicated as a dark cylinder. The filled circles on top show the completed strings and IceTop stations in February 2006, whereas the open circles correspond to additional finished IceTop stations. The figure is taken from Ref. [15].

Compared to the initial ratio (3.18) there is an excess of tau neutrinos and antineutrinos. It is anticipated that the IceCube neutrino observatory is able to detect this excess of high-energy tau neutrinos and antineutrinos by means of several different signatures [17]. The variety of signatures arises from the fact that a secondary tau lepton produced in a charged-current interaction of the primary cosmogenic tau neutrino/antineutrino, in which it obtains 0.75 times the tau neutrino/antineutrino energy E_ν in average, has a decay length of about 50 m per PeV.¹ Therefore, only tau events with tau energies E_τ up to 20 PeV can be fully contained in the IceCube detector. For higher energies, only the production vertex or the decay vertex of the tau is observable in the detector. The decay vertices can be of different kind, since the tau lepton can decay leptonically,

$$\tau^- \longrightarrow e^- + \bar{\nu}_e + \nu_\tau, \quad (4.2a)$$

$$\tau^- \longrightarrow \mu^- + \bar{\nu}_\mu + \nu_\tau, \quad (4.2b)$$

with branching ratios of $\sim 18\%$ and $\sim 17\%$, respectively, or hadronically with a branching ratio of $\sim 65\%$ [13]. For the antitau, we have respective decays with the same branching ratios. The possible signatures for different tau energies E_τ will be described in detail in the following. The distinction between tau-neutrino and tau-antineutrino events will be omitted from now on, since the tau-antineutrino events follow exactly the same principle as the described tau-neutrino events.

4.1.1 Double-bang signature

A double-bang signature denotes an event in which two separated showers are observed within the detector. The primary tau neutrino produces a tau lepton inside the detector volume by the reaction

$$\nu_\tau + N \longrightarrow \tau^- + X, \quad (4.3)$$

where N denotes a nucleon and X a hadronic shower, which is observed by the emittance of Cherenkov light. When the tau lepton decays to an electron, see Eq. (4.2a), or hadronically, it produces a second shower, an electromagnetic one in the first case and a hadronic one in the second. This means that the branching ratio for a double-bang event is $\sim 82\%$. For being distinguishable, the two showers, which are connected by the Cherenkov light trace of the tau lepton, must be separated by at least 100 m. The tau decay length is only larger than this distance if its energy E_τ is high enough. On the other hand, E_τ must not be too high in order to have both showers confined within the detector volume. These constraints give an acceptance range of the tau neutrino energy E_ν of approximately 2-20 PeV.

¹Recall 1 PeV = 10^{15} eV.

Signature	Branching ratio	E_ν energy acceptance
Double-bang	82 %	$\sim 2\text{-}20$ PeV
Lollipop	82 %	$\gtrsim 5$ PeV
Inverted-lollipop	100 %	$\gtrsim 5$ PeV
Sugardaddy	18 %	~ 5 PeV - 1 EeV

Table 4.1. Summary of the tau-neutrino and tau-antineutrino signatures which are expected to be accessible to the IceCube neutrino observatory.

4.1.2 Lollipop signature

If the primary neutrino interacts with a nucleon sufficiently far from the detector, the resulting shower cannot be observed. However, the produced tau lepton can enter the detector volume and there decay into a shower, as described in Sec. 4.1.1. The signature of the event in the detector is a Cherenkov light track entering the detector and ending in a shower, which is somewhat reminiscent of a lollipop. The track corresponds to the stick of the lollipop and the shower to the ball-shaped sweet part. The branching ratio of a lollipop event is, as in the case of a double-bang event, ~ 82 %. Requiring a minimal tau lepton decay length of 200 m the energy acceptance range is $E_\nu \gtrsim 5$ PeV.

4.1.3 Inverted-lollipop signature

As the name indicates, this is the inverse of the lollipop signature, i.e. the tau lepton is created inside the detector volume and then leaves the detector without further interaction. Thus, the detector signature consists of a shower followed by a Cherenkov light track leaving the detector. The branching ratio for this signature is 100 %, but possibly, there is background from muon neutrino charged-current events, since it is very hard to distinguish the initial shower and the created muon from the corresponding tau event. As for the lollipop signature, the energy acceptance range is $E_\nu \gtrsim 5$ PeV if we require a tau decay length of at least 200 m.

4.1.4 Sugardaddy signature

This signature is the complement to the lollipop signature. The tau lepton is created outside the detector such that the shower accompanying this reaction cannot be observed. Then, the tau enters the detector and decays into a muon which leaves the detector thereafter. This decay has a branching ratio of ~ 18 %. The resulting track in the detector does not have to be kinked at the location of the decay. However, the tau emits significantly less Cherenkov light than the subsequent muon. This is the reason

for the name Sugardaddy which is a lollipop with a cylindric sweet part (corresponding to the muon) on a stick (corresponding to the tau). For energies roughly between 1 PeV and 1 EeV,² the change in Cherenkov light intensity is expected to be large enough to be detectable by IceCube. Requiring the same 200 m tau decay length as before, the energy acceptance range of the sugardaddy signature is $E_\nu \gtrsim 5$ PeV and $E_\nu \lesssim 1$ EeV.

Table 4.1 summarizes the introduced tau-neutrino and tau-antineutrino signatures. The IceCube is expected to have event rates of 0.31 cosmogenic tau-neutrino/antineutrino events per year in the energy range from 0.1 PeV to 100 EeV [18] for the full configuration of 80 deployed in-ice strings. Thus, it is very likely that the IceCube experiment will be able to clearly identify events induced by cosmogenic tau neutrinos or antineutrinos in this energy range if neutrino oscillations are mass-difference driven.

²Recall 1 EeV = 10^{18} eV.

Chapter 5

Standard mass-difference neutrino oscillations and IceCube

Standard mass-difference (MD) neutrino oscillations are governed by the Hamiltonian (2.22) which shall be recalled here:

$$H_{\text{MD}} = \frac{1}{2E_\nu} U(\theta_{12}, \theta_{13}, \theta_{23}, \delta) \cdot \text{diag}(0, \Delta m_{21}^2, \Delta m_{31}^2) \cdot U^\dagger(\theta_{12}, \theta_{13}, \theta_{23}, \delta), \quad (5.1)$$

where E_ν is the neutrino energy, U the leptonic mixing matrix, θ_{ij} the neutrino mixing angles, Δm_{k1}^2 the neutrino mass-squared differences, and δ the CP-violating Dirac phase. This yields a neutrino-oscillation probability P_α^{MD} into neutrinos and antineutrinos of flavor α for the initial condition (3.18), i.e. for cosmogenic neutrinos and antineutrinos with $E_\nu > 10^{14}$ eV,

$$P_\alpha^{\text{MD}} = \frac{1}{3} \left[\left| U_{\alpha 1} U_{1e}^\dagger + U_{\alpha 2} \exp\left(-i\frac{\Delta m_{21}^2 L}{2E_\nu}\right) U_{2e}^\dagger + U_{\alpha 3} \exp\left(-i\frac{\Delta m_{31}^2 L}{2E_\nu}\right) U_{3e}^\dagger \right|^2 + 2 \left| U_{\alpha 1} U_{1\mu}^\dagger + U_{\alpha 2} \exp\left(-i\frac{\Delta m_{21}^2 L}{2E_\nu}\right) U_{2\mu}^\dagger + U_{\alpha 3} \exp\left(-i\frac{\Delta m_{31}^2 L}{2E_\nu}\right) U_{3\mu}^\dagger \right|^2 \right], \quad (5.2)$$

where L is the travel distance of the cosmogenic neutrinos/antineutrinos. This formula arises from the general MD neutrino-oscillation probability (2.8) and describes neutrino oscillations relevant to the IceCube experiment.

If an upper limit of E_ν of 10^{20} eV is assumed and it holds that

$$L \gg 100 \text{ pc}, \quad (5.3)$$

then the travel distance L is much larger than the oscillation lengths

$$L_{\text{osc},k1} = \frac{4\pi E_\nu}{\Delta m_{k1}^2}, \quad (5.4)$$

for $k \in \{2, 3\}$, and the difference $L_{\text{osc},31} - L_{\text{osc},21}$. Condition (5.3) is fulfilled for cosmogenic neutrinos and antineutrinos originating from outside our galaxy. In this case, Eq. (5.2) can be averaged over L and simplifies to

$$P_{\alpha}^{\text{MD}} = \frac{1}{3} \sum_{j=1}^3 \left(|U_{\alpha j} U_{j e}^{\dagger}|^2 + 2|U_{\alpha j} U_{j \mu}^{\dagger}|^2 \right). \quad (5.5)$$

For the neutrino mixing angles $\theta_{13} = 0$ and $\theta_{23} = \pi/4$, one obtains the neutrino-oscillation probabilities

$$P_e^{\text{MD}} = P_{\mu}^{\text{MD}} = P_{\tau}^{\text{MD}} = \frac{1}{3}, \quad (5.6)$$

which means that we expect to detect cosmogenic neutrinos and antineutrinos with $E_{\nu} > 10^{14}$ eV on Earth (approximately) in the ratio

$$N(\nu_e + \bar{\nu}_e) : N(\nu_{\mu} + \bar{\nu}_{\mu}) : N(\nu_{\tau} + \bar{\nu}_{\tau}) = 1 : 1 : 1, \quad (5.7)$$

for the present experimental values of θ_{13} and θ_{23} .

The occurrence of tau neutrinos and antineutrinos in (5.7) in contrast to the initial condition (3.18) is of importance. Since there are no other sources of these high-energy tau neutrinos and antineutrinos, the experimental observation of such a tau neutrino/antineutrino in the IceCube experiment would be potential evidence of MD neutrino oscillations.

Chapter 6

Nonstandard neutrino oscillations and IceCube

Nonstandard neutrino oscillations incorporate effects from new physics in addition to the established standard MD neutrino oscillations. The particular case of nonstandard neutrino oscillations which is considered here is based on the assumption that neutrinos have Fermi-point splitting (FPS), in analogy to the fermionic quasi-particles occurring in certain quantum gases of fermionic atoms at ultralow temperatures [19]. In such systems, a quantum phase transition between a vacuum state with fully-gapped fermionic spectrum and a vacuum state with Fermi points, i.e. points in three-momentum space at which the energy vanishes, is predicted. This phase transition occurs in the so-called BEC-BCS crossover region, where BEC stands for Bose-Einstein condensate and BCS for Bardeen, Cooper, and Schrieffer, i.e. the superconductive regime. Denoting two Fermi points in three-momentum space by \mathbf{b}_1 and \mathbf{b}_2 , we can define the splitting $\Delta\mathbf{b}_{21}$ between these two Fermi points:

$$\Delta\mathbf{b}_{21} \equiv \mathbf{b}_2 - \mathbf{b}_1. \quad (6.1)$$

We can carry over the concept of FPS to elementary particle physics. If neutrinos are assumed to have timelike FPS (in four-momentum space), it enters their dispersion laws in the following way

$$E_j \simeq p \pm b_0^{(j)} + \frac{m_j^2}{2p}, \quad (6.2)$$

for $j \in \{1, 2, 3\}$, where p denotes the neutrino momentum, $b_0^{(j)}$ the FPS parameters, and m_j the neutrino masses. Only for non-zero $b_0^{(j)}$, we can obtain $E_j = 0$ and as a result FPS. The altered dispersion relations result in the following extension of H_{MD} [20]:

$$\begin{aligned} H_{\text{MD+FPS}} = & \frac{1}{2E_\nu} U(\theta_{12}, \theta_{13}, \theta_{23}, \delta) \cdot \text{diag} (0, \Delta m_{21}^2, \Delta m_{31}^2) \cdot U^\dagger(\theta_{12}, \theta_{13}, \theta_{23}, \delta) \\ & + V(\chi_{12}, \chi_{13}, \chi_{23}, \omega) \cdot \text{diag} (0, \Delta b_0^{(21)}, \Delta b_0^{(31)}) \cdot V^\dagger(\chi_{12}, \chi_{13}, \chi_{23}, \omega), \end{aligned} \quad (6.3)$$

where the FPS part is parametrized by the matrix V , the FPS equivalent of the leptonic mixing matrix U , the angles χ_{ij} , the FPS differences $\Delta b_0^{(k1)} \equiv b_0^{(k)} - b_0^{(1)}$, and a complex phase ω . The relative phases between the MD and the FPS sector have been chosen to be zero. The domains of the FPS angles χ_{ij} and the FPS phase ω are in the limit $E_\nu \rightarrow \infty$

$$\chi_{ij} \in \left[0, \frac{\pi}{2}\right], \quad (6.4a)$$

$$\omega \in [0, 2\pi). \quad (6.4b)$$

If we denote the energy eigenvalues of $H_{\text{MD+FPS}}$ by $\epsilon_j \equiv \epsilon_j(E_\nu)$, for $j \in \{1, 2, 3\}$, the following energy-eigenvalue differences can be defined

$$\Delta\epsilon_{k1} \equiv \epsilon_k - \epsilon_1, \quad (6.5)$$

where $k \in \{2, 3\}$.

There exists a matrix W which diagonalizes $H_{\text{MD+FPS}}$. It is notable that, as the energy eigenvalues ϵ_j , this matrix W is dependent on E_ν . When FPS is incorporated, the neutrino-oscillation probability $P_\alpha^{\text{MD+FPS}}$ corresponding to that in Eq. (5.5) becomes

$$P_\alpha^{\text{MD+FPS}} = \frac{1}{3} \sum_{j=1}^3 \left(|W_{\alpha j} W_{j\epsilon}^\dagger|^2 + 2|W_{\alpha j} W_{j\mu}^\dagger|^2 \right). \quad (6.6)$$

This formula is valid if the following conditions hold true for the energy-eigenvalue differences $\Delta\epsilon_{k1}$:

$$|\Delta\epsilon_{k1}| L \gg 1, \quad (6.7a)$$

$$|\Delta\epsilon_{31} - \Delta\epsilon_{21}| L \gg 1. \quad (6.7b)$$

Since cosmogenic neutrinos and antineutrinos with energies $E_\nu > 10^{14}$ eV most likely originate from outside our galaxy, we will assume a lower limit on L of the order of one megaparsec. This assumption results in the conditions

$$|\Delta\epsilon_{k1}| \gg 10^{-29} \text{ eV}, \quad (6.8a)$$

$$|\Delta\epsilon_{31} - \Delta\epsilon_{21}| \gg 10^{-29} \text{ eV}. \quad (6.8b)$$

In the limit of low neutrino energies E_ν , the MD part in $H_{\text{MD+FPS}}$ dominates over the FPS part and the energy eigenvalues have the limits

$$\Delta\epsilon_{21} \rightarrow \frac{\Delta m_{21}^2}{2E_\nu}, \quad (6.9a)$$

$$\Delta\epsilon_{31} \rightarrow \frac{\Delta m_{31}^2}{2E_\nu}. \quad (6.9b)$$

Therefore, it results from the conditions (6.8a) and (6.8b) that the following must hold:

$$\frac{\Delta m_{k1}^2}{2E_\nu} \gg 10^{-29} \text{ eV}, \text{ for } k \in \{2, 3\}, \quad (6.10a)$$

$$\frac{1}{2E_\nu} (\Delta m_{31}^2 - \Delta m_{21}^2) \gg 10^{-29} \text{ eV}. \quad (6.10b)$$

This is the case for

$$E_\nu \ll 4 \times 10^{24} \text{ eV}, \quad (6.11)$$

an energy well above the highest observable energies of cosmogenic neutrinos and antineutrinos. Moreover, it has to hold that

$$\left| \Delta b_0^{(k1)} \right| \gg 10^{-29} \text{ eV}, \text{ } k \in \{2, 3\}, \quad (6.12a)$$

$$\left| \Delta b_0^{(31)} - \Delta b_0^{(21)} \right| \gg 10^{-29} \text{ eV}, \quad (6.12b)$$

since in the limit $E_\nu \rightarrow \infty$, the energy-eigenvalue differences $\Delta\epsilon_{k1}$ have the limits

$$\Delta\epsilon_{21} \rightarrow \Delta b_0^{(21)}, \quad (6.13a)$$

$$\Delta\epsilon_{31} \rightarrow \Delta b_0^{(31)}. \quad (6.13b)$$

Performing perturbation theory, one obtains the following behavior of the energy-eigenvalue differences $\Delta\epsilon_{k1}$ in first order of $\Delta m_{31}^2/(2E_\nu)$:

$$\begin{aligned} \Delta\epsilon_{21} \simeq \Delta b_0^{(21)} + \frac{\Delta m_{31}^2}{8E_\nu} & \left[\cos(2\chi_{12}) \left(2 \cos^2(\chi_{13}) + \sin(2\chi_{23}) (\cos(2\chi_{13}) - 3) \right) \right. \\ & \left. - 4 \sin(2\chi_{12}) \sin(\chi_{13}) \cos(2\chi_{23}) \cos(\omega) \right], \end{aligned} \quad (6.14a)$$

$$\begin{aligned} \Delta\epsilon_{31} \simeq \Delta b_0^{(31)} + \frac{\Delta m_{31}^2}{16E_\nu} & \left[(\cos(2\chi_{12}) + 3) \cos(2\chi_{13}) (\sin(2\chi_{23}) + 1) \right. \\ & + 2 \sin^2(\chi_{12}) (3 \sin(2\chi_{23}) - 1) \\ & \left. - 4 \sin(2\chi_{12}) \sin(\chi_{13}) \cos(2\chi_{23}) \cos(\omega) \right], \end{aligned} \quad (6.14b)$$

where terms of the order $\Delta m_{21}^2/(2E_\nu)$ are neglected and the standard MD neutrino-oscillation angles are chosen to be $\theta_{13} = 0$ and $\theta_{23} = \pi/4$. The energy corrections in Eqs. (6.14a) and (6.14b) can be positive as well as negative. Under certain circumstances, this results in an intersection of ϵ_1 and ϵ_2 at a specific energy E_I , i.e. the condition (6.8b) would not be fulfilled around this energy. However, the energy interval in which Eq. (6.6) would not be valid is very small if the conditions (6.12a) and (6.12b) apply.

We are interested in which way the inclusion of FPS can alter the standard MD neutrino-oscillation probabilities (5.6). Since the MD term in $H_{\text{MD}+\text{FPS}}$ is suppressed with rising neutrino energy E_ν , one preferably goes to high neutrino energies, in order to observe possible effects of FPS on neutrino oscillations. The IceCube experiment with its capability of detecting cosmogenic tau neutrinos and antineutrinos with $E_\nu > 10^{15}$ eV is a promising candidate for this task. Therefore, we will concentrate on FPS effects entering the tau neutrino-oscillation probability $P_\tau^{\text{MD}+\text{FPS}}$. However, the first thing which has to be investigated is the question when FPS has no or only very little effect on $P_\tau^{\text{MD}} = 1/3$. This can be determined in the limit $E_\nu \rightarrow \infty$ where the MD term in $H_{\text{MD}+\text{FPS}}$ is completely suppressed. Then, the tau neutrino-oscillation probability becomes

$$P_\tau^{\text{FPS}} = \frac{1}{3} \sum_{j=1}^3 \left(|V_{\tau j} V_{j e}^\dagger|^2 + 2|V_{\tau j} V_{j \mu}^\dagger|^2 \right). \quad (6.15)$$

Figures 6.1-6.4 show the regions in the phase space of χ_{12} , χ_{13} , and χ_{23} for which $P_\tau^{\text{FPS}} > 0.3$, i.e. a maximal decrease of 10 % with respect to P_τ^{MD} . The phase ω is set to a different value in each figure, namely $\omega = 0$, $\omega = \pi/3$, $\omega = 2\pi/3$, and $\omega = \pi$.¹ The figures indicate that the regions in the FPS parameter space for which FPS effects do not decrease the tau neutrino-oscillation probability significantly concentrate around

$$\chi_{23} \simeq \frac{\pi}{4}, \quad (6.16)$$

as long as $\chi_{13} < \pi/4$. This includes the combination

$$\chi_{12} = 0.58, \quad \chi_{13} = 0, \quad \chi_{23} = \frac{\pi}{4}, \quad (6.17)$$

which corresponds to the standard MD neutrino-oscillation case. For larger values of χ_{13} , χ_{23} can obtain arbitrary values. However, the point

$$\chi_{12} = \chi_{23} = \frac{\pi}{4} \quad (6.18)$$

is no longer allowed, as it is the case as long as χ_{13} is small. It should also be noted that a significant enhancement of the tau neutrino-oscillation probability is not possible. It holds that

$$P_\tau^{\text{FPS}} < 0.35. \quad (6.19)$$

Thus, for the phase space regions shown in Figs. 6.1-6.4, $P_\tau^{\text{MD}+\text{FPS}}$ does not deviate much from the standard value of 1/3 except for a constrained E_ν interval where possible interference effects between the MD term and the FPS term in $H_{\text{MD}+\text{FPS}}$ are dominant.

¹It is sufficient to consider $\omega \in [0, \pi]$, since P_τ^{FPS} is symmetric in ω , as it will be shown in Eq. (6.37).

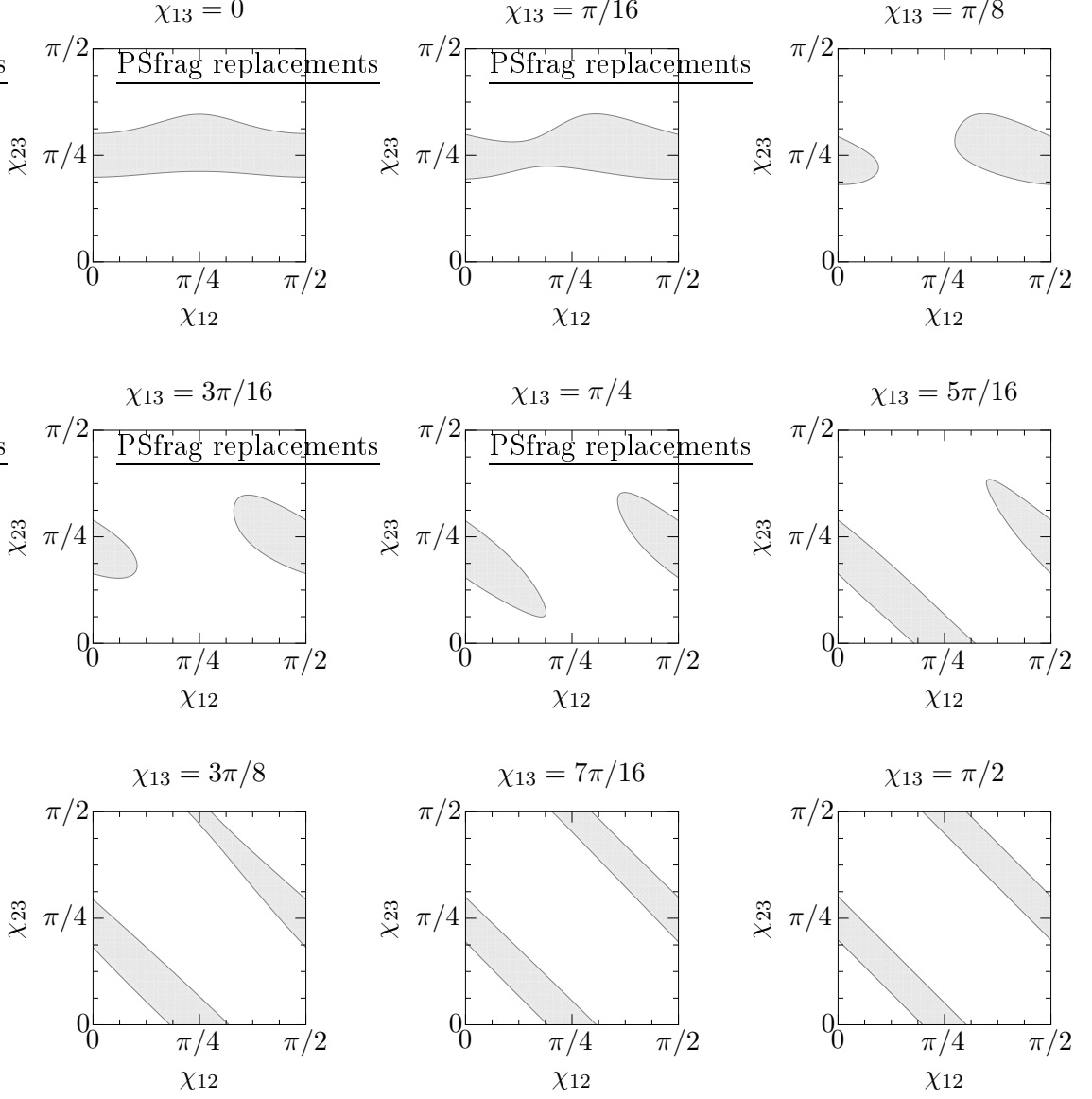


Figure 6.1. Slices in the χ_{12} - χ_{23} plane for which $P_\tau^{\text{FPS}} > 0.3$ is fulfilled. Different slices correspond to different values of χ_{13} . The phase ω is set to $\omega = 0$.

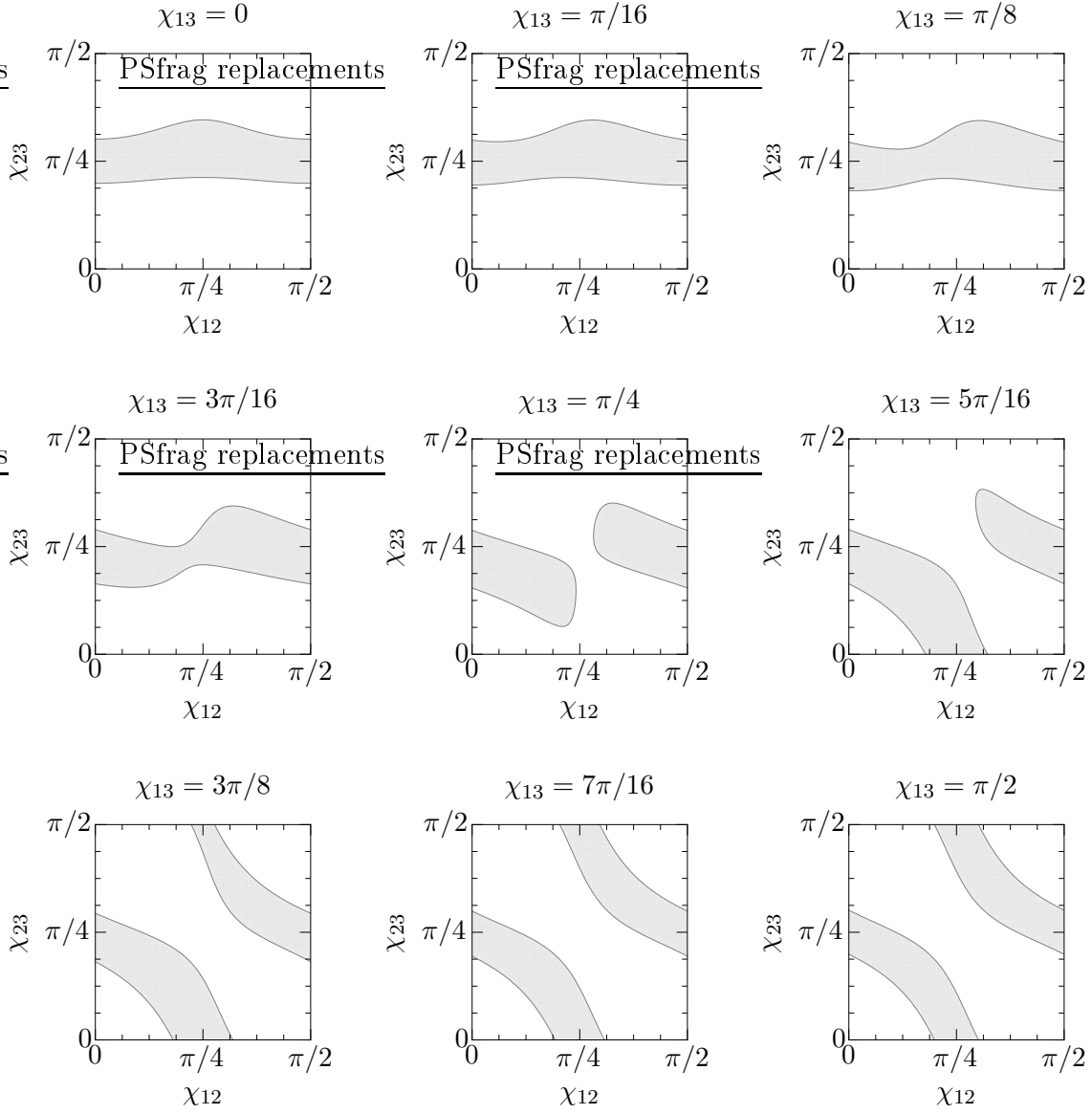


Figure 6.2. Slices in the χ_{12} - χ_{23} plane for which $P_{\tau}^{\text{FPS}} > 0.3$ is fulfilled. Different slices correspond to different values of χ_{13} . The phase ω is set to $\omega = \pi/3$.

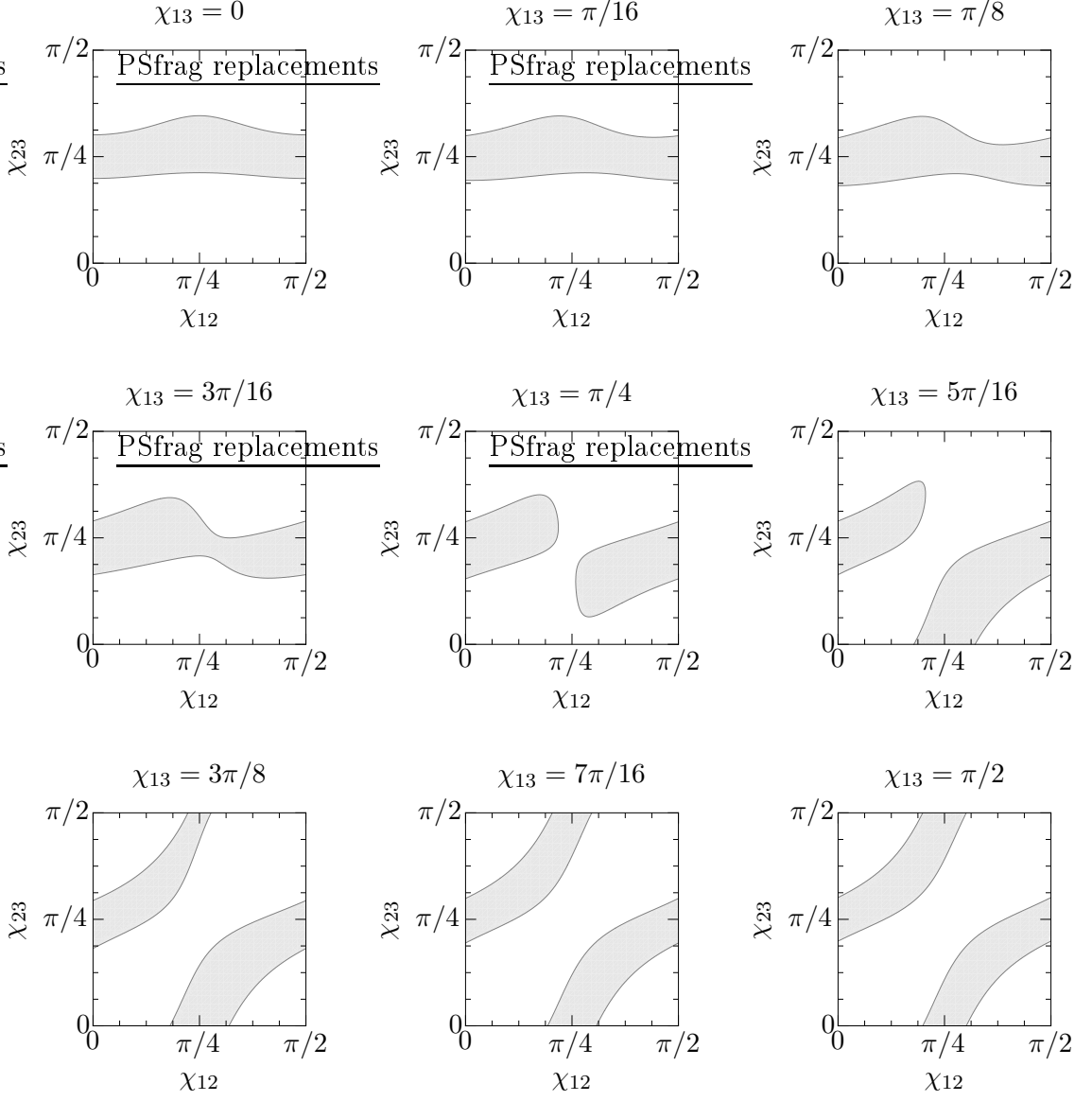


Figure 6.3. Slices in the χ_{12} - χ_{23} plane for which $P_\tau^{\text{FPS}} > 0.3$ is fulfilled. Different slices correspond to different values of χ_{13} . The phase ω is set to $\omega = 2\pi/3$.

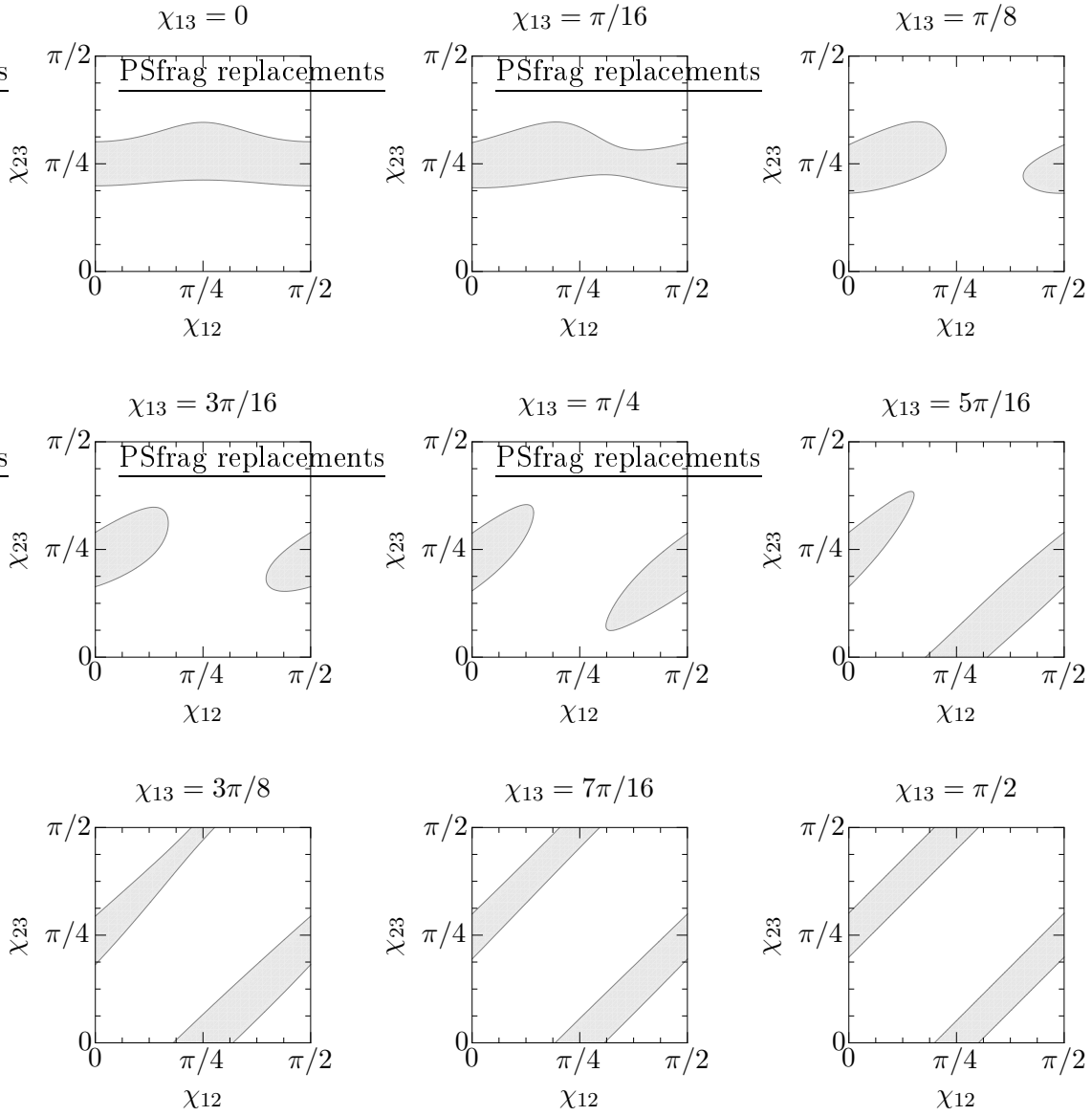


Figure 6.4. Slices in the χ_{12} - χ_{23} plane for which $P_{\tau}^{\text{FPS}} > 0.3$ is fulfilled. Different slices correspond to different values of χ_{13} . The phase ω is set to $\omega = \pi$.

$P(P_\tau^{\text{FPS}} > 0.3) = 0.24$
$P(P_\tau^{\text{FPS}} < 0.15) = 0.25$
$P(P_\tau^{\text{FPS}} < 0.075) = 0.10$

Table 6.1. Numerical values of the probability that P_τ^{FPS} stays above or falls below certain thresholds P_t .

We would like to estimate the probabilities for different cases of FPS altering the tau neutrino-oscillation probability. Since we basically know nothing about the values of χ_{12} , χ_{13} , χ_{23} , and ω , we will assume each point in the parameter space as equally probable. Then, the probability for P_τ^{FPS} staying above or falling below a threshold P_t is given by

$$P(P_\tau^{\text{FPS}} \gtrless P_t) = \frac{\int_0^\pi \int_0^{\frac{\pi}{2}} \int_0^{\frac{\pi}{2}} \int_0^{\frac{\pi}{2}} d\omega d\chi_{12} d\chi_{13} d\chi_{23} \Theta(\pm P_\tau^{\text{FPS}} \mp P_t)}{\pi \left(\frac{\pi}{2}\right)^3}, \quad (6.20)$$

where Θ is the Heaviside step function and $\pi(\pi/2)^3$ is the volume of the whole parameter space. $P(P_\tau^{\text{FPS}} < P_t)$ is also a measure for the probability that an experiment, which is able to distinguish the case $P_\tau^{\text{FPS}} < P_t$ from the standard MD neutrino-oscillation case, detects effects from FPS. Numerical results for different values of P_t are given in Table 6.1. There is a 24 % chance that P_τ^{FPS} stays above 0.3, which corresponds to the previously discussed case. The probability is 25 % for FPS altering the tau neutrino-oscillation probability significantly ($P_\tau^{\text{FPS}} < 0.15$). For a dramatic alteration of the tau neutrino-oscillation probability ($P_\tau^{\text{FPS}} < 0.075$), there is a chance of 10 %. This means that, in principal, there is quite a large probability for possible FPS effects being observable in the oscillations of high-energy cosmogenic neutrinos.

The case including a dramatic alteration of the tau neutrino-oscillation probability is the most interesting one, in particular when

$$P_\tau^{\text{FPS}} = 0. \quad (6.21)$$

This is fulfilled if there is no connection between the ν_e - ν_μ sector and ν_τ in the FPS part of $H_{\text{MD+FPS}}$, i.e. if the following two conditions hold

$$\Delta b_0^{(21)} V_{e2} V_{2\tau}^\dagger + \Delta b_0^{(31)} V_{e3} V_{3\tau}^\dagger = 0, \quad (6.22a)$$

$$\Delta b_0^{(21)} V_{\mu 2} V_{2\tau}^\dagger + \Delta b_0^{(31)} V_{\mu 3} V_{3\tau}^\dagger = 0, \quad (6.22b)$$

which is the case for certain regions in the FPS parameter space, particularly

$$\chi_{13} = 0, \quad (6.23a)$$

$$\chi_{23} = 0, \quad (6.23b)$$

with χ_{12} and ω being arbitrary.

As a concrete example, we will consider the case of no mixing in the FPS sector which is very similar to quark mixing. This corresponds to the following standard MD neutrino-oscillation and FPS parameters:

$$\begin{aligned} \theta_{12} = 0.58, \quad \theta_{13} = 0, \quad \theta_{23} = \pi/4, \\ \Delta m_{21}^2 = 7.9 \times 10^{-5} \text{ eV}^2, \quad \Delta m_{31}^2 = 2.6 \times 10^{-3} \text{ eV}^2, \quad \delta = 0, \end{aligned} \quad (6.24a)$$

$$\begin{aligned} \chi_{12} = 0, \quad \chi_{13} = 0, \quad \chi_{23} = 0, \\ \Delta b_0^{(21)} = 5 \times 10^{-18} \text{ eV}, \quad \Delta b_0^{(31)} = 10^{-17} \text{ eV}, \quad \omega = 0, \end{aligned} \quad (6.24b)$$

where the standard MD neutrino-oscillation parameters (6.24a) are chosen according to present experimental results [21]. The choice of the FPS differences $\Delta b_0^{(k1)}$ is motivated as follows. Let us first define $\Delta b_0^{(31)}$ to be the larger FPS difference. Then, the FPS part in $H_{\text{MD+FPS}}$ dominates over the standard MD part if

$$\frac{\Delta m_{31}^2}{2E_\nu} < \Delta b_0^{(31)}. \quad (6.25)$$

For the chosen value of $\Delta b_0^{(31)}$, this condition is fulfilled if

$$E_\nu \gtrsim 10^{14} \text{ eV}. \quad (6.26)$$

Therefore, it is expected that in the considered case, $P_\tau^{\text{MD+FPS}}$ significantly deviates from the standard MD value of 1/3 in this energy domain. Since a case with $P_\tau^{\text{FPS}} = 0$ is considered, we assume that

$$P_\tau^{\text{MD+FPS}} \rightarrow 0, \quad (6.27)$$

if the FPS part is at least one order of magnitude larger than the standard MD part, i.e.

$$10 \frac{\Delta m_{31}^2}{2E_\nu} < \Delta b_0^{(31)}. \quad (6.28)$$

For the chosen value of $\Delta b_0^{(31)}$, this results in an energy range

$$E_\nu \gtrsim 10^{15} \text{ eV}, \quad (6.29)$$

which corresponds to the total energy acceptance range of the IceCube tau-neutrino and tau-antineutrino events described in Sec. 4.1.

The energy-eigenvalue differences $\Delta\epsilon_{k1}$ of the considered example are shown in Fig. 6.5. Equations (6.14a) and (6.14b) yield for the chosen parameters

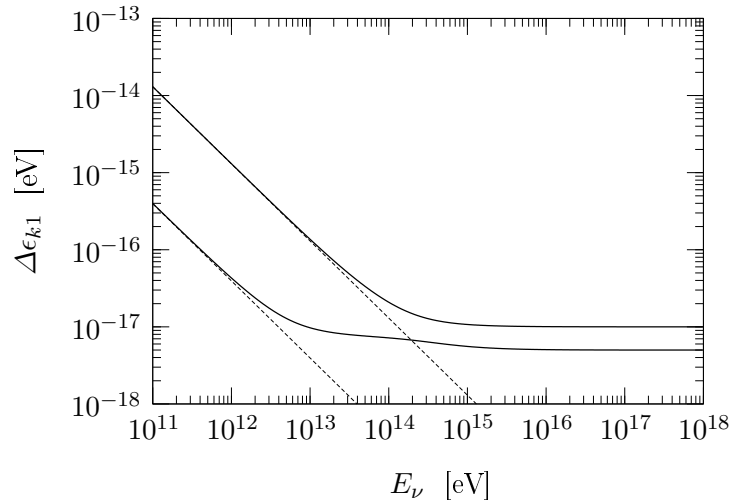


Figure 6.5. Energy-eigenvalue differences $\Delta\epsilon_{k1}$, $k \in \{2, 3\}$, for the standard MD neutrino-oscillation parameters (6.24a) and the FPS parameters (6.24b). The dashed lines show the eigenvalues of the standard MD neutrino-oscillation mechanism $\Delta m_{k1}^2/(2E_\nu)$, $k \in \{2, 3\}$.

$$\Delta\epsilon_{21} \simeq \Delta b_0^{(21)} + \frac{\Delta m_{31}^2}{4E_\nu} + \mathcal{O}\left(\left(\Delta m_{31}^2/(2E_\nu)\right)^2\right), \quad (6.30a)$$

$$\Delta\epsilon_{31} \simeq \Delta b_0^{(31)} + \frac{\Delta m_{31}^2}{4E_\nu} + \mathcal{O}\left(\left(\Delta m_{31}^2/(2E_\nu)\right)^2\right). \quad (6.30b)$$

This suggests that $\Delta\epsilon_{21}$ and $\Delta\epsilon_{31}$ grow monotonically with decreasing E_ν . Figure 6.5 also shows that the conditions (6.8a) and (6.8b) are fulfilled and that for high energies, as it was anticipated previously, one obtains the limits

$$\Delta\epsilon_{21} \rightarrow \Delta b_0^{(21)}, \quad (6.31a)$$

$$\Delta\epsilon_{31} \rightarrow \Delta b_0^{(31)}, \quad (6.31b)$$

as well as for low energies

$$\Delta\epsilon_{21} \rightarrow \frac{\Delta m_{21}^2}{2E_\nu}, \quad (6.32a)$$

$$\Delta\epsilon_{31} \rightarrow \frac{\Delta m_{31}^2}{2E_\nu}. \quad (6.32b)$$

The resulting energy dependence of $P_\tau^{\text{MD+FPS}}$ is shown in Fig. 6.6.² For energies below 10^{14} eV, it resembles the standard MD neutrino-oscillation case with a value of

²Although Eq. (6.6) is only valid for $E_\nu > 10^{14}$ eV the energy range in Fig. 6.6 is extended to 10^{12} eV for illustration purposes.

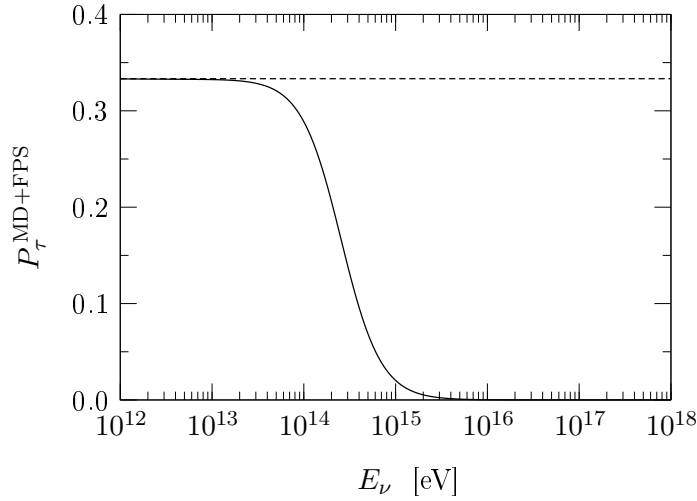


Figure 6.6. Neutrino-oscillation probability $P_\tau^{\text{MD+FPS}}$, as defined by (6.6), for the standard MD neutrino-oscillation parameters (6.24a) and the FPS parameters (6.24b). The dashed line shows the standard MD neutrino-oscillation probability $P_\tau^{\text{MD}} = 1/3$.

1/3. For energies larger than 10^{14} eV, the probability decreases rapidly, approaching zero at around 10^{15} eV, as it was anticipated previously.

We will now consider a second example which is similar to the previous one, but it incorporates large mixing in the FPS sector. Therefore, only the FPS mixing angles χ_{12} , χ_{13} , and χ_{23} are changed compared to the preceding case. The particular choice of standard MD neutrino-oscillation and FPS parameters is as follows:

$$\begin{aligned} \theta_{12} = 0.58, \quad \theta_{13} = 0, \quad \theta_{23} = \pi/4, \\ \Delta m_{21}^2 = 7.9 \times 10^{-5} \text{ eV}^2, \quad \Delta m_{31}^2 = 2.6 \times 10^{-3} \text{ eV}^2, \quad \delta = 0, \end{aligned} \quad (6.33a)$$

$$\begin{aligned} \chi_{12} = 0, \quad \chi_{13} = \pi/4, \quad \chi_{23} = \pi/2, \\ \Delta b_0^{(21)} = 5 \times 10^{-18} \text{ eV}, \quad \Delta b_0^{(31)} = 10^{-17} \text{ eV}, \quad \omega = 0. \end{aligned} \quad (6.33b)$$

The resulting energy-eigenvalue differences $\Delta\epsilon_{k1}$ are shown in Fig. 6.7. They show very similar behavior as in the previous example which is suggested by the results of Eqs. (6.14a) and (6.14b)

$$\Delta\epsilon_{21} \simeq \Delta b_0^{(21)} + \frac{\Delta m_{31}^2}{8E_\nu} + \mathcal{O}\left(\left(\frac{\Delta m_{31}^2}{2E_\nu}\right)^2\right), \quad (6.34a)$$

$$\Delta\epsilon_{31} \simeq \Delta b_0^{(31)} + \mathcal{O}\left(\left(\frac{\Delta m_{31}^2}{2E_\nu}\right)^2\right). \quad (6.34b)$$

Here, the second order correction of ϵ_2 , being the largest energy-eigenvalue difference, is positive.

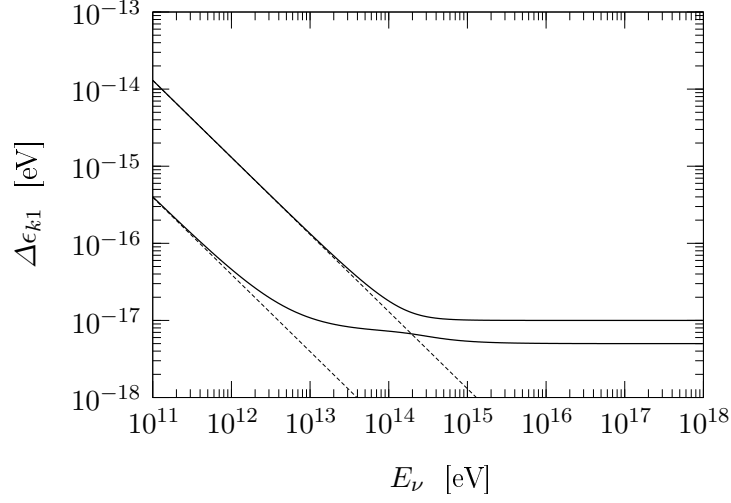


Figure 6.7. Energy-eigenvalue differences $\Delta\epsilon_{k1}$, $k \in \{2, 3\}$, for the standard MD neutrino-oscillation parameters (6.33a) and the FPS parameters (6.33b). The dashed lines show the eigenvalues of the standard MD neutrino-oscillation mechanism $\Delta m_{k1}^2/(2E_\nu)$, $k \in \{2, 3\}$.

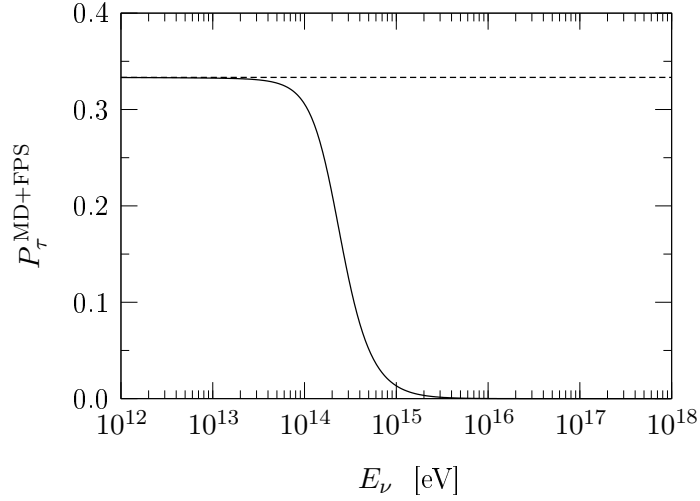


Figure 6.8. Neutrino-oscillation probability $P_\tau^{\text{MD+FPS}}$, as defined by (6.6), for the standard MD neutrino-oscillation parameters (6.33a) and the FPS parameters (6.33b). The dashed line shows the standard MD neutrino-oscillation probability $P_\tau^{\text{MD}} = 1/3$.

The energy dependence of $P_\tau^{\text{MD+FPS}}$ is shown in Fig. 6.8. Since the choice $\chi_{12} = 0$, $\chi_{13} = \pi/4$, and $\chi_{23} = \pi/2$ fulfills, as in the case of all three angles being zero, the conditions (6.22a) and (6.22a), $P_\tau^{\text{MD+FPS}}$ behaves very similar to the previous example. For energies below 10^{14} eV, it resembles the standard MD neutrino-oscillation case with a value of $1/3$. Above 10^{14} eV, the probability decreases rapidly and approaches zero at around 10^{15} eV.

What do the preceding considerations imply for the IceCube experiment? It has been shown that it depends on the mixing in the FPS sector, i.e. the values obtained by χ_{12} , χ_{13} , and χ_{23} , whether FPS can or cannot affect the results of the IceCube experiment compared to the case of standard MD neutrino oscillations. However, if the FPS mixing angles have the appropriate values, the tau neutrino-oscillation probability drops to zero for sufficiently high neutrino energies E_ν . More quantitatively, according to Eq. (6.28), we have as condition for $P_\tau^{\text{MD+FPS}} \simeq 0$

$$E_\nu \gtrsim 5 \frac{\Delta m_{31}^2}{\Delta b_0^{(31)}}. \quad (6.35)$$

Putting in the concrete values of Δm_{31}^2 and $\Delta b_0^{(31)}$ chosen before this yields

$$E_\nu \gtrsim 10^{15} \text{ eV}. \quad (6.36)$$

This energy range corresponds to the complete energy acceptance range of tau-neutrino and tau-antineutrino events in the IceCube experiment described in Sec. 4.1. Thus, the IceCube experiment would not observe any of the discussed tau-neutrino or tau-antineutrino events at energies above 10^{15} eV in contrast to the expectations arising from the predictions of the standard MD neutrino-oscillation mechanism.

The absence of tau-neutrino and tau-antineutrino events at energies above 10^{15} eV would suggest that there are nonstandard contributions to neutrino oscillations, possibly from FPS. However, the experimental verification of this scenario is a complicated task, since statistics in the relevant energy region is expected to be poor for the IceCube experiment (see Sec. 4.1). Better statistics would help here. Moreover, better statistics could make it possible to distinguish between the standard MD neutrino-oscillation case and a less dramatic alteration of the neutrino-oscillation probability by FPS. This is favorable, since a scenario fulfilling $P_\tau^{\text{FPS}} < 0.15$ is far more probable than a scenario for which a very small value of P_t as upper limit is demanded (see Table 6.1).

In the cases discussed, the FPS differences were chosen of the order of 10^{-17} eV. This is the lower limit for the FPS differences, in order to obtain no tau-neutrino or tau-antineutrino events at energies above 10^{15} eV. Present bounds on the FPS differences are of the order of 10^{-13} eV - 10^{-14} eV [22]. The IceCube experiment is therefore sensitive to FPS differences which are at least three orders of magnitude smaller than the present bounds.

Another matter of interest is the question how the results of the IceCube experiment can be influenced by the FPS phase ω . The terms in P_τ^{FPS} which depend on ω can be summarized as

$$P_\tau^{\text{FPS},\omega} = \frac{1}{6} \left[\frac{1}{2} \sin(4\chi_{12}) \sin(\chi_{13}) \left((1 + \sin^2(\chi_{13})) \sin(4\chi_{23}) - \cos^2(\chi_{13}) \sin(2\chi_{23}) \right) \cos(\omega) - \sin^2(2\chi_{12}) \sin^2(\chi_{13}) \sin^2(2\chi_{23}) \cos(2\omega) \right]. \quad (6.37)$$

The variation of this quantity can only be of significant size if χ_{13} is not too small. In addition, the possible choices for the other two angles χ_{12} and χ_{23} are also restricted. A suitable and not too unrealistic combination of the mixing angles is

$$\chi_{12} = \frac{\pi}{8}, \quad \chi_{13} = \frac{\pi}{4}, \quad \chi_{23} = \frac{\pi}{8}. \quad (6.38)$$

Then, the variation of $P_\tau^{\text{FPS},\omega}$ is

$$P_\tau^{\text{FPS},\omega=0} - P_\tau^{\text{FPS},\omega=\pi} = \frac{3\sqrt{2}-1}{24} \simeq 0.14, \quad (6.39)$$

which coincides with the variation of $P_\tau^{\text{MD+FPS}}$ in the limit $E_\nu \rightarrow \infty$. Figure 6.9 shows the neutrino-oscillation probability $P_\tau^{\text{MD+FPS}}$ for the following choice of standard MD neutrino-oscillation and FPS parameters:

$$\theta_{12} = 0.58, \quad \theta_{13} = 0, \quad \theta_{23} = \pi/4, \quad (6.40a)$$

$$\Delta m_{21}^2 = 7.9 \times 10^{-5} \text{ eV}^2, \quad \Delta m_{31}^2 = 2.6 \times 10^{-3} \text{ eV}^2, \quad \delta = 0,$$

$$\chi_{12} = \pi/8, \quad \chi_{13} = \pi/4, \quad \chi_{23} = \pi/8, \quad (6.40b)$$

$$\Delta b_0^{(21)} = 5 \times 10^{-18} \text{ eV}, \quad \Delta b_0^{(31)} = 10^{-17} \text{ eV}.$$

The difference between the case $\omega = 0$ and $\omega = \pi$ is considered. For $\omega = 0$, there is only an insignificant deviation from the standard MD case throughout the complete energy range. However, for $\omega = \pi$, $P_\tau^{\text{MD+FPS}}$ starts to drop at an energy $E_\nu \simeq 10^{14}$ eV and falls to a value of about 0.18 for $E_\nu \gtrsim 10^{16}$ eV. The difference between both curves at high energies coincides very well with the difference computed in Eq. (6.39).

It has been shown that a non-zero phase ω , i.e. the existence of CP violation in the FPS sector, can alter the neutrino-oscillation probability $P_\tau^{\text{MD+FPS}}$ quite significantly. In the considered example, $P_\tau^{\text{MD+FPS}}$ is almost equal to the standard MD neutrino-oscillation case for $\omega = 0$ and decreases to almost half of the standard MD value at energies $E_\nu \gtrsim 10^{15}$ eV for $\omega = \pi$. However, it has to be emphasized that a non-zero ω can only alter $P_\tau^{\text{MD+FPS}}$ significantly for a quite restricted range of values of

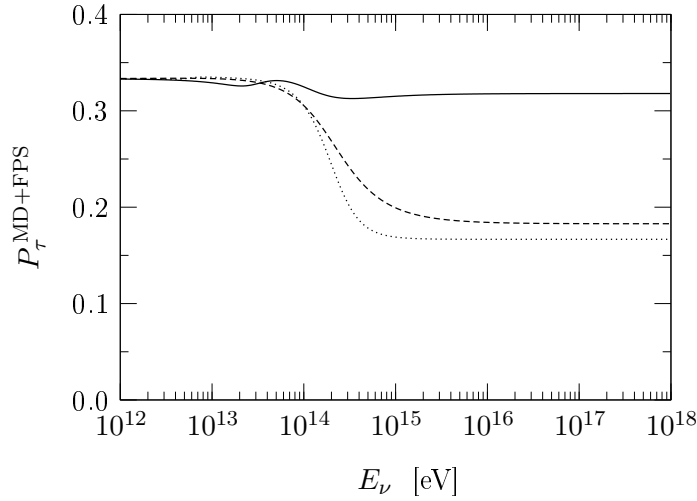


Figure 6.9. Neutrino-oscillation probability $P_{\tau}^{\text{MD+FPS}}$, as defined by (6.6), for the standard MD neutrino-oscillation parameters (6.40a) and the FPS parameters (6.40b). The solid line corresponds to $\omega = 0$ and the dashed line to $\omega = \pi$. The dotted line shows $P_{\tau}^{\text{MD+FPS}}$ for the same standard MD neutrino-oscillation parameters and $\chi_{12} = 0$, $\chi_{13} = \pi/4$, $\chi_{23} = 0$, and $\omega = 0$.

χ_{12} , χ_{13} , and χ_{23} . In particular, χ_{13} must not be small. Moreover, it is not clear if the IceCube experiment is able to discriminate between, e.g., the full and half of the number of expected tau-neutrino and tau-antineutrino events at energies above 10^{15} eV. This problem could be overcome by better statistics, e.g. by an experiment with a larger detector volume than IceCube.

However, if IceCube or any other similar experiment should be able to clearly identify a deficiency of these tau-neutrino and tau-antineutrino events, there is no possibility to tell whether this deficiency arises from a non-zero phase ω or another combination of FPS mixing angles with $\omega = 0$. This is illustrated in Fig. 6.9, where the case with FPS angles $\chi_{12} = 0$, $\chi_{13} = \pi/4$, and $\chi_{23} = 0$ and vanishing phase ω is shown for comparison. This issue could only be overcome by complementary experiments, e.g. experiments which measure neutrino oscillations at high energies dependent on the propagation distance L rather than averaged oscillations. Summing up, it has to be said that possible CP violation in the FPS sector can alter the results of the IceCube experiment, but it is not possible for the IceCube experiment to make a statement if there is or if there is not CP violation in the FPS sector.

Chapter 7

Conclusion

Ultrahigh-energy cosmic rays with energies between 10^{17} and 3×10^{20} eV have been measured in experiments. These cosmic rays can scatter off cosmic microwave background photons, a process known as the Greisen–Zatsepin–Kuzmin mechanism. Moreover, similar scattering processes take place which involve other cosmic backgrounds, in particular the cosmic ultraviolet-optical and infrared backgrounds. In these scattering processes, photopions are created and in the decay of these photopions, electron neutrinos, muon neutrinos, and tau neutrinos along with the corresponding antineutrinos are produced in the ratio one to two to zero in very good approximation. This neutrino production mechanism is the dominating one for all cosmogenic neutrinos and antineutrinos with energies above 10^{14} eV.

The absence of initially created tau neutrinos and antineutrinos is of particular importance, since mass-difference neutrino oscillations alter the neutrino-flavor composition to equal fractions of all flavors during neutrino propagation. The IceCube Neutrino Observatory is expected to be able to measure the resulting excess of cosmogenic tau neutrinos and antineutrinos with energies above 10^{14} eV by means of several unique signatures, which are sensitive to energies greater than 10^{15} eV. The observation of these cosmogenic tau neutrinos and antineutrinos would be interpreted as further evidence for the existence of mass-difference neutrino oscillations.

In this work, neutrino oscillations have been discussed which include nonstandard contributions arising from Fermi-point splitting. It has been considered which effect these nonstandard neutrino oscillations have on the results of the IceCube experiment. In particular, a formula has been derived which describes neutrino oscillations involving Fermi-point splitting. This formula is valid for minimal neutrino propagation lengths of one megaparsec, which is a small distance on cosmological scales.

It has been shown that Fermi-point splitting can alter the oscillation probability of cosmogenic tau neutrinos and antineutrinos in such a way that no tau neutrinos or antineutrinos with energies above 10^{15} eV arrive on Earth (see Figs. 6.6 and 6.8). As a result, the IceCube experiment would not observe any of the events induced by

these tau neutrinos or antineutrinos. This would then suggest that contributions from Fermi-point splitting could be present in neutrino oscillations.

The sensitivity of the IceCube experiment to contributions from Fermi-point splitting allows values of the Fermi-point splittings which are at least three orders of magnitude below present bounds. However, its sensitivity is restricted to limited combinations of the mixing angles and the phase in the Fermi-point splitting sector. This issue could be overcome by, e.g., a successor of the IceCube experiment with better statistics, which would extend the sensitivity to a larger fraction of the space of the Fermi-point splitting mixing angles and the Fermi-point splitting phase. This extension would imply a larger probability that effects from Fermi-point splitting can be observed. See Table 6.1 for a quantitative estimate. Table 6.1 also shows that there is a relatively large principal probability for being able to detect possible effects from Fermi-point splitting in the oscillations of high-energy cosmogenic neutrinos.

Effects from possible CP violation in the Fermi-point splitting sector may be observable at the IceCube experiment (see Fig. 6.9). However, a definite result on the presence of CP violation in the Fermi-point splitting sector cannot be expected from IceCube. This has to wait for complementary experimental data, e.g. from other neutrino-oscillation experiments with very high neutrino energies but, in contrast to the IceCube experiment, well-defined neutrino propagation distance.

Appendix A

GZK kinematics

We want to derive a formula for the kinematics of the GZK processes, in which a proton and a photon produce a Δ^+ . This problem is effectively two+one-dimensional and the conservation equations of energy and momentum are given by

$$\begin{pmatrix} E_p \\ \sqrt{E_p^2 - m_p^2} \\ 0 \end{pmatrix} + \begin{pmatrix} E_\gamma \\ E_\gamma \cos \theta \\ E_\gamma \sin \theta \end{pmatrix} = \begin{pmatrix} \sqrt{p_{\Delta^+,x}^2 + p_{\Delta^+,y}^2 + m_{\Delta^+}^2} \\ p_{\Delta^+,x} \\ p_{\Delta^+,y} \end{pmatrix}, \quad (\text{A.1})$$

where E_p is the proton energy, m_p the proton mass, E_γ the photon energy, θ the angle between the momenta of the initial proton and photon, m_{Δ^+} the Δ^+ mass, and $p_{\Delta^+,x}$ and $p_{\Delta^+,y}$ the Δ^+ momentum in x and y direction, respectively. The momentum of the proton is chosen to point in x direction. Inserting the equations for $p_{\Delta^+,x}$ and $p_{\Delta^+,y}$ into the energy conservation equation and subsequent squaring yields

$$(E_p + E_\gamma)^2 = E_p^2 - m_p^2 + E_\gamma^2 \cos^2 \theta + 2\sqrt{E_p^2 - m_p^2} E_\gamma \cos \theta + E_\gamma^2 \sin^2 \theta + m_{\Delta^+}^2, \quad (\text{A.2})$$

and this simplifies to

$$2 E_p E_\gamma = m_{\Delta^+}^2 - m_p^2 + 2 \left(E_p - \frac{m_p^2}{2E_p} \right) E_\gamma \cos \theta, \quad (\text{A.3})$$

where $\sqrt{E_p^2 - m_p^2}$ has been Taylor expanded to first order in m_p^2 . Sorting the terms with respect to powers of E_p gives

$$2(1 - \cos \theta) E_\gamma E_p^2 - (m_{\Delta^+}^2 - m_p^2) E_p + m_p^2 E_\gamma \cos \theta = 0. \quad (\text{A.4})$$

The last term can be neglected and we obtain as result for the proton energy E_p

$$E_p = \frac{m_{\Delta^+}^2 - m_p^2}{2E_\gamma(1 - \cos \theta)}. \quad (\text{A.5})$$

Bibliography

- [1] B. Pontecorvo, *Mesonium and antimesonium*, Sov. Phys. JETP **6**, 429 (1957).
- [2] B. Pontecorvo, *Inverse beta processes and nonconservation of lepton charge*, Sov. Phys. JETP **7**, 172 (1958).
- [3] Z. Maki, M. Nakagawa and S. Sakata, *Remarks on the unified model of elementary particles*, Prog. Theor. Phys. **28**, 870 (1962).
- [4] J. Gluza and M. Zralek, *Parameters' domain in three flavour neutrino oscillations*, Phys. Lett. **B517**, 158 (2001), [hep-ph/0106283](#).
- [5] K. Greisen, *End to the cosmic-ray spectrum?*, Phys. Rev. Lett. **16**, 748 (1966).
- [6] G. T. Zatsepin and V. A. Kuzmin, *Upper limit of the spectrum of cosmic rays*, JETP Lett. **4**, 78 (1966).
- [7] D. Allard *et al.*, *Cosmogenic neutrinos from the propagation of ultra high energy nuclei*, JCAP **0609**, 005 (2006), [astro-ph/0605327](#).
- [8] A. M. Hillas, *The origin of ultra-high-energy cosmic rays*, Ann. Rev. Astron. Astrophys. **22**, 425 (1984).
- [9] M. Roth, for the Auger Collaboration, *Measurement of the UHECR energy spectrum using data from the Surface Detector of the Pierre Auger Observatory*, (2007), [arXiv:0706.2096](#) [[astro-ph](#)].
- [10] Pierre Auger Collaboration, J. Abraham *et al.*, *Correlation of the highest energy cosmic rays with nearby extragalactic objects*, Science **318**, 939 (2007), [arXiv:0711.2256](#) [[astro-ph](#)].
- [11] M. G. Hauser and E. Dwek, *The cosmic infrared background: measurements and implications*, Ann. Rev. Astron. Astrophys. **39**, 249 (2001), [astro-ph/0105539](#).
- [12] T. Hahn, *Generating Feynman diagrams and amplitudes with FeynArts 3*, Comput. Phys. Commun. **140**, 418 (2001), [hep-ph/0012260](#).

- [13] Particle Data Group, W. M. Yao *et al.*, *Review of particle physics*, J. Phys. **G33**, 1 (2006).
- [14] V. S. Beresinsky and G. T. Zatsepin, *Cosmic rays at ultra high energies (neutrino?)*, Phys. Lett. **B28**, 423 (1969).
- [15] P. O. Hulth for the IceCube Collaboration, *From AMANDA to IceCube*, (2006), astro-ph/0604374.
- [16] *IceCube: Project timeline*, available at <http://www.icecube.wisc.edu/science/timeline.php> (2007).
- [17] D. F. Cowen for the IceCube Collaboration, *Tau neutrinos in IceCube*, J. Phys. Conf. Ser. **60**, 227 (2007).
- [18] A. Ishihara for the IceCube Collaboration, *The EHE neutrino search capability of the IceCube observatory*, Nucl. Phys. Proc. Suppl. **165**, 200 (2007), astro-ph/0611794.
- [19] F. R. Klinkhamer and G. E. Volovik, *Quantum phase transition for the BEC-BCS crossover in condensed matter physics and CPT violation in elementary particle physics*, JETP Lett. **80**, 389 (2004), cond-mat/0407597.
- [20] F. R. Klinkhamer, *Possible new source of T and CP violation in neutrino oscillations*, Phys. Rev. **D73**, 057301 (2006), hep-ph/0601116.
- [21] M. Maltoni *et al.*, *Status of global fits to neutrino oscillations*, New J. Phys. **6**, 122 (2004), hep-ph/0405172.
- [22] M. C. Gonzalez-Garcia and M. Maltoni, *Atmospheric neutrino oscillations and new physics*, Phys. Rev. **D70**, 033010 (2004), hep-ph/0404085.

Acknowledgments

First of all, I would like to thank Prof. Klinkhamer for supervising my Diplomarbeit and for many helpful suggestions.

I also have to thank Prof. Drexlin for accepting the Korreferat.

Furthermore, I thank Mareike Haberichter, Elisabeth Kant, Marco Schreck, and Markus Schwarz for proof-reading and many useful comments.

All members of the ITP deserve my thanks for the nice atmosphere and many interesting discussions.

Finally, I would like to thank my parents and all persons who are close to me for their support and their confidence.

Zusammenfassung

Neutrinooszillationen beschreiben das Verhalten von Neutrinos während ihrer Propagation. Ein Neutrino, das mit einem bestimmten Flavor erzeugt wurde, muss nicht notwendiger Weise mit demselben Flavor vorgefunden werden, nachdem es eine gewisse Strecke propagiert ist. Vielmehr gibt es eine endliche Wahrscheinlichkeit, es mit einem anderen Flavor vorzufinden. Dies ist darauf zurückzuführen, dass die drei Flavorzustände, nämlich ν_e , ν_μ und ν_τ , nicht die Neutrino-Eigenzustände sind. Folglich sind die Flavorzustände Linearkombinationen der Eigenzustände. Man spricht hier von Mischung. Diese wird von drei Mischwinkeln und einer CP-verletzenden Phase beschrieben.

Im Standardbild, das man von Neutrinooszillationen (im Vakuum) hat, entsprechen die Neutrino-Eigenzustände den Zuständen mit wohldefinierter Masse. Für Neutrinooszillationen ist hier notwendig, dass mindestens zwei Neutrinomassen von null verschieden und nicht entartet sind. Da die Neutrinooszillationswahrscheinlichkeit in diesem Fall von der Differenz der Massenquadrate abhängt, nennt man diese Art der Oszillationen Massendifferenz-Neutrinooszillationen. Die daraus resultierenden Ergebnisse für die Neutrinooszillationswahrscheinlichkeiten stimmen sehr gut mit den Messungen bisheriger Neutrinooszillationsexperimente überein. Deswegen wird dieses Modell als die Standardbeschreibung für Neutrinooszillationen betrachtet.

Neben den durch rein Massendifferenzen induzierten Neutrinooszillationen gibt es verschiedene Modelle, die dieses Konzept erweitern. Die in dieser Arbeit betrachtete Form der Erweiterung basiert auf dem Konzept der sogenannten Fermipunkt-Aufspaltung. Man nimmt an, dass Neutrinos in Analogie zu den fermionischen Quasiteilchen, die in gewissen Quantengasen bei ultraniedrigen Temperaturen auftreten, Fermipunkt-Aufspaltungen haben. Dies führt zu einem zusätzlichen Term (neben dem Term, der die Massendifferenzen beinhaltet) im Hamilton-Operator, der Neutrinooszillationen beschreibt. Je nach Größenordnung der Fermipunkt-Aufspaltung im Vergleich zu den Massendifferenzen können zusätzliche Effekte in Neutrinooszillationen auftreten.

Es ist von Interesse, wie man experimentell mögliche Effekte von Fermipunkt-Aufspaltung messen kann. Dazu geht man vorzugsweise zu hohen kinetischen Energien der Neutrinos, da Massendifferenz induzierte Neutrinooszillationen mit zunehmender Neutrinoenergie unterdrückt werden. Effekte, die aus Fermipunkt-Aufspaltung resultieren, sind jedoch von der Neutrinoenergie unabhängig.

Die höchsten Neutrinoenergien, die uns bekannt sind, trifft man bei Neutrinos kosmischen Ursprungs an. Bei ihrer Erzeugung spielen extrem hochenergetische kosmische Strahlen die tragende Rolle. Kosmische Strahlen extrem hoher Energie können an Photonen der kosmischen Mikrowellen-Hintergrundstrahlung streuen. Dieser Prozess wird Greisen-Zatsepin-Kuzmin-Mechanismus genannt. Darüber hinaus finden ähnliche Streuprozesse statt, die kosmische Hintergrundstrahlung anderer Wellenlängen einbeziehen. Dies betrifft insbesondere die kosmische ultraviolett-optische und Infrarot-Hintergrundstrahlung.

In den Streuprozessen, die an Photonen verschiedener kosmischer Hintergrundstrahlungen stattfinden, werden Δ^+ -Resonanzen erzeugt, die unter anderem in sogenannte Photopionen zerfallen. Diese Photopionen zerfallen weiter und erzeugen dabei Neutrinos und Antineutrinos. Elektronenneutrinos, Myonneutrinos und Tauneutrinos werden zusammen mit den entsprechenden Antineutrinos im Verhältnis eins zu zwei zu null gebildet. Dies gilt in sehr guter Näherung. Die angesprochenen Prozesse sind die primäre Quelle für alle Neutrinos und Antineutrinos kosmischen Ursprungs mit Energien größer als 10^{14} eV.

Das Fehlen von Tauneutrinos und -antineutrinos als Produkt dieser Streuprozesse ist von besonderer Relevanz. Massendifferenz-Neutrinooszillationen verändern das anfängliche Verhältnis der verschiedenen Neutrinoarten hin zu gleichen Anteilen aller Flavours. Dies bedeutet einen Überschuss an Tauneutrinos und -antineutrinos kosmischen Ursprungs mit Energien größer als 10^{14} eV, der auf der Erde messbar sein sollte. Ein Nachweis dieses Überschusses würde als weiterer Beleg für die Existenz von Massendifferenz-Neutrinooszillationen gesehen werden.

Das IceCube-Neutrinoobservatorium ist ein derzeitiges Neutrinoexperiment, das sich am Südpol befindet. Es benutzt das antarktische Eis als Detektormaterial und wird in fertig ausgebautem Zustand ein Detektorvolumen in der Größenordnung eines Quadratkilometers haben. In das polare Eis sind Photovervielfacherröhren an Strängen vertikal äquidistant eingelassen. Dabei bilden die Stränge mit Photovervielfacherröhren, insgesamt sollen es 80 an der Zahl werden, von oben betrachtet ein großes sechseckiges Gitter. Bis Anfang 2007 waren 22 Stränge installiert, die Fertigstellung des Experimentes ist für jenseits des Jahres 2010 geplant.

Das IceCube-Experiment wird den Erwartungen zufolge in der Lage sein, den Überschuss an Tauneutrinos und -antineutrinos kosmischen Ursprungs mit Energien größer als 10^{14} eV nachweisen zu können. Dies ist mit Hilfe verschiedener eindeutiger Signaturen möglich, die für Energien größer 10^{15} eV sensitiv sind. Die Größenordnung dieser Neutrinoenergien macht das IceCube-Experiment zu einem viel versprechenden Werkzeug, um Neutrinooszillationen auf mögliche Effekte eines erweiterten Neutrinooszillationsmodelles zu überprüfen.

In dieser Arbeit werden wie oben erwähnt Neutrinooszillationen basierend auf einem erweiterten Modell, das Fermipunkt-Aufspaltung beinhaltet, betrachtet. Dabei wird analysiert, inwieweit mögliche Effekte dieser Fermipunkt-Aufspaltung durch das IceCube-

Experiment messbar sind. Hierzu wurde eine Formel hergeleitet, die die Neutrinooszillationswahrscheinlichkeit mit einbezogener Fermipunkt-Aufspaltung beschreibt. Diese Formel ist für eine minimale durch die Neutrinos zurückgelegte Wegstrecke von einem Megaparsec gültig, was eine kleine Distanz im Hinblick auf kosmologische Größenordnungen ist.

Resultierend wurde gezeigt, dass Fermipunkt-Aufspaltung die Oszillationswahrscheinlichkeit von Tauneutrinos und -antineutrinos kosmischen Ursprungs dahingehend abändern kann, dass keine Tauneutrinos oder -antineutrinos mit Energien größer als 10^{15} eV auf der Erde gelangen. In diesem Fall würde das IceCube-Experiment keines der Ereignisse, die von diesen Tauneutrinos und -antineutrinos herrühren, beobachten. Dies würde dann darauf hindeuten, dass Fermipunkt-Aufspaltung einen Beitrag zu Neutrinooszillationen liefert. Das IceCube-Experiment ist dabei empfindlich für Werte der Fermipunkt-Aufspaltung, die mindestens drei Größenordnungen unterhalb bisheriger Schranken liegen.

Die Empfindlichkeit des IceCube-Experiments gegenüber Fermipunkt-Aufspaltung ist jedoch beschränkt auf gewisse Kombinationen der Mischungswinkel und der Phase im Bereich der Fermipunkt-Aufspaltung. Diese Problematik könnte zum Beispiel durch ein Nachfolgeexperiment von IceCube gelöst werden, das über bessere Statistik verfügen würde. Dies würde die Empfindlichkeit auf einen größeren Teil des Parameterraumes der Mischungswinkel und der Phase im Sektor der Fermipunkt-Aufspaltung erweitern und hätte eine höhere Wahrscheinlichkeit zur Folge, dass Effekte der Fermipunkt-Aufspaltung beobachtbar wären.

Effekte möglicher CP-Verletzung im Bereich der Fermipunkt-Aufspaltung sind unter Umständen vom IceCube-Experiment beobachtbar. Ein eindeutiges Ergebnis darüber, ob CP-Verletzung im Sektor der Fermipunkt-Aufspaltung vorliegt, kann vom IceCube-Experiment jedoch nicht erwartet werden. Hierzu sind komplementäre experimentelle Resultate erforderlich, zum Beispiel von anderen Neutrinooszillationsexperimenten mit sehr hohen Neutrinoenergien aber im Gegensatz zum IceCube-Experiment eindeutig definierter Propagationsstrecke der Neutrinos.